

RSC Advances



This is an *Accepted Manuscript*, which has been through the Royal Society of Chemistry peer review process and has been accepted for publication.

Accepted Manuscripts are published online shortly after acceptance, before technical editing, formatting and proof reading. Using this free service, authors can make their results available to the community, in citable form, before we publish the edited article. This *Accepted Manuscript* will be replaced by the edited, formatted and paginated article as soon as this is available.

You can find more information about *Accepted Manuscripts* in the [Information for Authors](#).

Please note that technical editing may introduce minor changes to the text and/or graphics, which may alter content. The journal's standard [Terms & Conditions](#) and the [Ethical guidelines](#) still apply. In no event shall the Royal Society of Chemistry be held responsible for any errors or omissions in this *Accepted Manuscript* or any consequences arising from the use of any information it contains.

Multiple pulse spin locking in nanofluids

Gregory B. Furman*, Shaul D. Goren, Victor M. Meerovich, Vladimir L. Sokolovsky

*Physics Department, Ben Gurion University of the Negev,
Beer Sheva, 84105 Israel Email:gregoryf@bgu.ac.il (G.B.Furman)*

Abstract

We study the multiple pulse spin locking dynamics of the nuclear spins in a liquid or a gas entrapped in nanosized cavities. Two cases are considered when the cavities in orientational order and isotropically disordered. The spins inside the cavities are coupled by the dipole-dipole interaction with the same interaction constant. It is shown that, under the high temperature approximation, in a spin system, irradiated by multiple pulse sequence, the quasi-equilibrium state is established. An analytical expression is obtained describing the dependence of the steady-state magnetization on the structural parameters of a nanocavity and the characteristics of a gas or a liquid confined in nanocavities. The relaxation process which follows the establishment of equilibrium is considered. For the case of orientationally ordered cavities, the analytical expression for the relaxation time is derived. When the nanocavities are isotropically disordered, the time dependence of the magnetization is numerically calculated. As shown for this case, the relaxation process is characterized by two time constants differing by two orders of magnitude.

An advantage of the application of the multiple pulse spin locking measurement method over the NMR cryoporometry technique is that the measurements of magnetization and its relaxation, along with the information about the cavity size, allow determining the shape and orientation of the nanocavity.

I. INTRODUCTION

Nuclear magnetic resonance (NMR) has become a powerful analytical tool in the study of structure and dynamic properties of molecules (both organic and inorganic) in solutions, liquid crystals, and solids, and compound environments such as membranes [1–3].

Over the past two decades it was becoming increasingly clear that the NMR technique is very applicable tool for studying soft matter systems such as nanostructures and nanoporous materials [4–6]. Based on a significant difference in magnetic and non-magnetic properties of the material enclosed in nanocavities, several methods for studying the structure of these materials have been proposed [7–14]. Molecular geometries can be derived from cross-relaxation rates which depend on the internuclear distance due to spin-spin interactions, such as the dipole-dipole interactions (DDI) between nuclear spins [4–6]. In isotropic liquids the secular dipole-dipole coupling essentially vanishes, but it is still possible to use the non-secular dipole-dipole coupling by the way of their effect on the relaxation of the spin system [1–3].

Various NMR techniques, ranging from cryoporometry technique [14], spin locking [15], spin dynamics in a local field [16, 17], multiple-quantum NMR [18–22] to spin-relaxation experiments [6, 23], were used to identify and quantify finite size effects. Nanoporous materials have found wide application, from gas separations in the petrochemical industry to air or water purification and using in medicine like controlled drug delivery.

The feature of the NMR spectroscopy which makes it so useful for chemical and structural analysis of liquids and solutions is high resolution allowing one to observe extremely weak interactions such as the interaction of nuclear spins with magnetic fields induced by orbital motions of electrons which leads to the chemical shift. These weak interactions are sensitive to the local properties of environment and may be used as a determinative method for characterizing environment. However, in solids, sufficiently strong DDI "covers" these weaker interaction and do not allow one using the last interactions to specify the environment.

The idea of coherent averaging of strong interactions, such as DDI, for the purpose of narrowing NMR spectral line has been spawned various high-resolution NMR techniques for solids. Of particular interest has been the development of methods of suppressing the effects of homonuclear dipolar broadening and thus obtaining high resolution NMR spectra of solids. One of the most effective and promising techniques is the multiple-pulse radio-frequency (RF) irradiation, application of which can increase by several orders the sensitivity

of the NMR method in the study of weak interactions in solids [24, 25]. The multiple-pulse NMR can provide a much higher data rate because the NMR signal can be sampled between the RF pulses and the relaxation curve is recorded during one scan. Accordingly, the spin-lock experiment may yield information about slowly fluctuating processes [24, 25].

However, most of studies using the multipulse RF NMR methods deal with the spin dynamics of a nuclear spin system in bulk solid. To our best knowledge, the multiple-pulse NMR methods were not applied to study the spin dynamics and spin-spin and spin-lattice relaxations in gases or liquids confined to nanoscale volumes such as nanopores and nanocavities. Motivation of application of multiple-pulse NMR methods in the study of nanoscale structures can be explained by the fact that in gases or liquids the intermolecular DDI between nuclear spins are not averaged to zero [26], as usually happens in bulk gases or in isotropic liquids [27]. Only very weak long-range residual DDI do not vanish in liquids [8]. The measurement of residual long-range dipolar coupling can potentially provide unique information on structured media [10]. The difference between the long-range DDI and DDI in nanoscale materials is that the latter is characterized by a single universal dipolar coupling constant which depends on the volume, shape of the nanocavity and its orientation relatively to the external magnetic field [26, 28–30]. This dependence can be used to obtain useful information on the structure of nanosized objects from the NMR experiments [31].

In this paper we consider the multiple spin locking dynamics and spin lattice relaxation in liquids or gases entrapped in nanosized cavities (Fig.1). We investigate two cases. In the first case, the material is in orientational order when the cavities are oriented along a common direction, their long axis, a , see Fig. 1 (a). In the second case, the material is isotropically disordered, as schematically illustrated in Fig. 1 (b).

This paper is organized as follows. In section II, for the convenience of the reader, we describe the procedure of averaging in coordinate and spin spaces. In section III, we consider a quasi-equilibrium state and steady-state magnetization. In section IV, the evolution of the spin system during multiple-pulse spin locking is analyzed. The last section is the conclusion.

II. AVERAGING OF THE DIPOLE-DIPOLE HAMILTONIAN IN COORDINATE AND SPIN SPACES

Largely the possibility of extraction of the structural and dynamic parameters from the NMR experiments is based on averaging of spin motion in the coordinate and the spin spaces. Part of this averaging occurs quite naturally, for example, averaging in coordinate of the dipole-dipole interactions in liquid samples. An example of averaging in the spin space is truncation of the internal spin-spin interaction Hamiltonians of spin systems in high magnetic fields.

For an adequate description of a spin system restricted by a cavity and irradiated by a multiple pulse RF sequence, the Hamiltonian should be averaged in both coordinate and spin spaces.

A. Averaging in coordinate space

Let us consider a system of N nuclear spins, $I = 1/2$, enclosed in an elongated cavity with the principal axes a , b , and $c = b$; an external field H_0 is directed along the z -axis (Fig. 1). The dipole-dipole Hamiltonian of a spin system in the external magnetic field can be separated into the two parts: one of them is a secular part with respect to I_z (I_z is the projection of the spin angular momentum operators \vec{I} on the z -axis) and the second is a non-secular part. The secular part of the DDI Hamiltonian is given by [1, 32]

$$H_d = - \sum_{i < j} \frac{\gamma^2 \hbar}{r_{ij}^3} P_2(\cos \theta_{ij}) \left(3I_{zi}I_{zj} - \vec{I}_i \vec{I}_j \right), \quad (1)$$

where γ is the gyromagnetic ratio, $P_2(\cos \theta_{ij}) = \frac{1}{2}(3 \cos^2 \theta_{ij} - 1)$, $\vec{I}_i \vec{I}_j = \sum_{\mu} I_{i\mu} I_{j\mu}$ and $I_{j\mu}$ is the projection of the angular momentum operator of the j -th spin ($j = 1, 2, \dots, N$) on the μ -axis ($\mu = x, y, z$), θ_{ij} is the angle between the z -axis and the radius-vector \vec{r}_{ij} from the i -th to the j -th spins.

For bulk gases or liquids, molecular diffusion [1, 33] causes practical vanishing of the averaged DDI Hamiltonian [34]. Actually, the averaged value of the intensity of interactions depends on the angle θ_{ij} as $P_2(\cos \theta_{ij})$. The averaged value of this quantity over angle θ_{ij} is

$$\text{zero: } \bar{P}_2(\cos \theta_{ij}) = \int_0^{\pi} P_2(\cos \theta_{ij}) \sin \theta_{ij} d\theta_{ij} = 0.$$

In contrast to bulk gases or liquids, in nanosized cavities, molecules of a gas or a liquid are subjected to restricted diffusion, but still move randomly throughout the whole cavity, from one cavity wall to another, during a time t_{mov} which is much less than the NMR time scale, $t_{mov} \ll t_{NMR}$ [26, 28–30, 35]. As a result, the averaged value of $P_2(\cos\theta_{ij})$ can be not zero. Let us estimate the characteristic size l of a nanocavity containing water at which the condition $t_{mov} \ll t_{NMR}$ is fulfilled. The diffusion coefficient of water molecules can be estimated by using the Einstein-Stokes equation. The diffusion coefficient for spherical particles moving through a liquid, $D = \frac{k_B T}{6\pi\sigma\lambda}$, where k_B is the Boltzmann's constant, T is the absolute temperature, $\sigma = 8.94 \times 10^{-4} \frac{Ns}{m^2}$ is the dynamic viscosity and $\lambda = 2 \times 10^{-10}$ m is the molecular van der Waals radius [36]. Within framework of this hydrodynamic model, we estimate $D \approx 2 \times 10^{-9} \frac{m^2}{s}$ that is close to the experimental value $D \approx 2.299 \times 10^{-9} \frac{m^2}{s}$ at 25°C [37].

The typical NMR time scale which characterizes the flip-flop transition is $t_{NMR} = \left(\frac{\gamma^2 \hbar}{r^3}\right)^{-1} \simeq 10^{-5}$ s. Therefore, the averaged DDI Hamiltonian can be non-zero if the typical length l of the water-confined cavity is much less than $\sqrt{2Dt_{NMR}} \simeq 200$ nm. Then, taking into account the ergodic theorem [26, 28, 29], the spin evolution in a nanosize cavity can be described by the averaged DDI Hamiltonian

$$\bar{H}_d = G \sum_{i < j} \left(3I_{zi}I_{zj} - \vec{I}_i \vec{I}_j \right) \quad (2)$$

with the space-averaged pair coupling G for any pair of the i -th and j -th spins [28, 29]

$$G = -\frac{\gamma^2 \hbar}{V} P_2(\cos\theta) F(\varepsilon), \quad (3)$$

where V is the cavity volume and $F(\varepsilon)$ is the form-factor depending monotonically on the ratio $\varepsilon = \frac{a}{b}$: $\lim_{\varepsilon \rightarrow \infty} (F(\varepsilon)) = \frac{2\pi}{3}$, $\lim_{\varepsilon \rightarrow 0} (F(\varepsilon)) = -\frac{4\pi}{3}$, and $\lim_{\varepsilon \rightarrow 1} (F(\varepsilon)) = 0$ [26], θ denotes the orientation of the cavity with respect to the external magnetic field, \vec{H}_0 (Fig. 1c). Note, that for spherical cavities $\varepsilon = 1$ and $F(\varepsilon) = 0$, and hence, averaging the DDI Hamiltonian gives zero, as in the case of a bulk liquid. The averaged DDI Hamiltonian (2) can be rewritten in the following form [29]

$$\bar{H}_d = \frac{G}{2} \left(3I_z^2 - \vec{I}^2 \right), \quad (4)$$

where $\vec{I}^2 = I_x^2 + I_y^2 + I_z^2$ is the square of the total nuclear spin operator and $I_\mu = \sum_i I_{\mu i}$ is the operator of the projection of the total spin operator onto the μ -axis ($\mu = x, y, z$).

B. Averaging in spin space

Evolution of a spin system containing nuclear spins I entrapped in a nanosized cavity and irradiated by a RF pulse train $\left(\frac{\pi}{2}\right)_y - \frac{t_c}{2} - (\varphi_l - t_c)^k$ (here φ_l denotes the pulse which rotates spins through an angle φ around the l -axis, t_c is the time interval between the pulses) can be described by a solution of the following equation for the density matrix $\rho(t)$:

$$\frac{d\rho(t)}{dt} = [\mathcal{H}(t), \rho(t)], \quad (5)$$

with the Hamiltonian

$$\mathcal{H}(t) = \mathcal{H}_0 + \mathcal{H}_{RF}(t) + \bar{H}_d. \quad (6)$$

Here \mathcal{H}_0 is the Zeeman energy

$$\mathcal{H}_0 = -\omega_0 I_z \quad (7)$$

represents the interaction of the spin system with an external magnetic field \vec{H}_0 directed along the z -axis and $\omega_0 = \gamma H_0$. $\mathcal{H}_{RF}(t)$ gives the action of the RF field on the spin system:

$$\mathcal{H}_{RF}(t) = \gamma H_1 \left(\vec{l} \vec{I} \right) f(t) \cos \omega t \quad (8)$$

where H_1 and ω , are the amplitude and frequency of a RF field pulse, \vec{l} is the unit vector along direction of the RF field, $f(t)$ is the pulse function that describes the pattern of the RF-field pulses:

$$f(t) = \frac{t_w}{t_c} \sum_{k=0}^{\infty} \delta\left(\frac{t}{t_c} - k - 1\right), \quad (9)$$

t_w is the duration of the pulse. Without loss of generality, we can assume that $\omega = \omega_0$ and $\vec{l} = \{1, 0, 0\}$.

To solve Eq. (5), we apply the unitary transformation

$$\tilde{\rho}(t) = U(t) e^{-it\mathcal{H}_0} \rho(t) e^{it\mathcal{H}_0} U^\dagger(t) \quad (10)$$

with the unitary operator

$$U(t) = \exp\left\{-i\omega_e I_x \int_0^t dt' [f(t') - 1]\right\} \quad (11)$$

where $\omega_e = \frac{\gamma H_1 t_w}{t_c}$ is the magnitude of the effective field.

Eq. (5) for the density matrix after transformation (10) can be rewritten as

$$\frac{d\tilde{\rho}(t)}{dt} = [\tilde{\mathcal{H}}(t), \tilde{\rho}(t)], \quad (12)$$

where

$$\tilde{\mathcal{H}}(t) = \omega_e I_x + \mathcal{H}_{dx}^{(0)} + \phi_2(t) \mathcal{H}_d^{(2)} + \phi_{-2}(t) \mathcal{H}_d^{(-2)}, \quad (13)$$

are $\phi_m(t)$ is the periodic function with the period t_c

$$\phi_m(t) = \exp \left\{ im\omega_e \int_0^t dt' [f(t') - 1] \right\}, \quad m = \pm 2, \quad (15)$$

$\mathcal{H}_{dx}^{(0)}$ is the secular part ($[\mathcal{H}_{dx}^{(0)}, \omega_e I_x] = 0$)

$$\mathcal{H}_{dx}^{(0)} = -\frac{G}{4} (3I_x^2 - I^2) \quad (16)$$

and $\mathcal{H}_d^{(m)}$ is the non-secular part ($[\mathcal{H}_d^{(m)}, \omega_e I_x] = m\omega_e \mathcal{H}_d^{(m)}$)

$$\mathcal{H}_d^{(\pm m)} = -\frac{3G}{8} \sum_{ij} I_i^\pm I_j^\pm. \quad (17)$$

where I_i^+ and I_i^- are the raising and lowering spin angular momentum operators of the i -th spin.

To account for the time-dependent terms in equation (13), we expand the periodic functions $\phi_m(t)$ (15) in the Fourier series:

$$\phi_m(t) = \sum_{n=-\infty}^{\infty} c_n^{(m)} e^{-i\omega_n t}, \quad \phi_m(t) = \phi_{-m}^*(t), \quad \omega_n = \frac{2\pi n}{t_c}, \quad (18)$$

where

$$c_n^{(\pm 2)} = \frac{(-1)^n \sin(2\varphi)}{n\pi + 2\varphi} \quad (19)$$

and $\varphi = \omega_e t_c$.

In the case where $\omega_e \simeq \omega_{loc}$, ($\omega_{loc} = \frac{1}{2}G\sqrt{3(N-1)}$ is the local dipolar field [19]), the Hamiltonian (13) can be divided into two parts:

$$\tilde{\mathcal{H}}(t) = \mathcal{H}_{eff} + Q(t), \quad (20)$$

where

$$\mathcal{H}_{eff} = \omega_e I_x + c_0^0 \mathcal{H}_{dx}^{(0)} + \frac{\sin(2\varphi)}{2\varphi} (\mathcal{H}_d^{(2)} + \mathcal{H}_d^{(-2)}) \quad (21)$$

is a sum of the time-independent terms and

$$Q(t) = \sum_{n=-\infty, n \neq 0}^{\infty} e^{-i\omega_n t} (c_n^{(2)} \mathcal{H}_d^{(2)} + c_n^{(-2)} \mathcal{H}_d^{(-2)}) \quad (22)$$

is the time-dependent term.

Similarly to consideration of multiple pulse technique in bulk solid NMR [38–40], we apply the perturbation theory which, in the first approximation, takes into account only the time-independent Hamiltonian (21). Note that, when φ approaches to zero, the Hamiltonian (21) coincides with the Hamiltonians for spin systems irradiated by a continuous RF magnetic field providing spin locking in bulk solids [32] and nanocavities [15].

The effective Hamiltonian (21) describes a dipolar coupled spin system of liquid or gas in a cavity under an effective magnetic field with the amplitude $\omega_e \simeq \omega_{loc}$.

Below we analyze the characteristics of the considered spin system basing on the structure of hydrogenated amorphous silicon a-Si:H with nano-cavities of $\sim 45 \text{ nm}^3$ containing H_2 at 2 kbar ($N \sim 600$) [26, 41].

Fig. 2 presents the dependences of the local dipolar field ω_{loc} on angle θ and volume V (Fig. 2a), on angle θ and number of spins N (Fig. 2b), on angle θ and form factor F (Fig.2c), and on volume V and form factor F (Fig.2d).

In the case of gas, the number of spins and the cavity volume are independent values and the local field decreases with increase of volume as $1/V$ (Fig. 2a). For a liquid with the constant spin density, $\frac{N}{V}$, the local field decreases as $1/\sqrt{V}$. The local dipolar field can be practically regarded as a negligible quantity in experiments with the liquid at $\omega_{loc} \leq 100 \text{ Hz}$ which corresponds to the volume of about 600 nm^3 .

The absolute value of the local field reaches its maxima at $\theta = 0$ and $\theta = \pi$ (parallel and antiparallel to the external DC magnetic field) and at $\theta = \frac{\pi}{2}$ (perpendicular to this field). Note, that at

$$\cos \theta = \pm \frac{1}{\sqrt{3}} \quad (23)$$

the local dipolar field vanishes (Fig. 2). Eq. (23) has two solutions: $\theta_{mag} = 54.74^\circ$ (which is known as "the magic angle" [32] for bulk solids) and $\theta = 125.26^\circ$. At these angles the first approximation for the local magnetic field gives zero.

In the range of angles from $\theta = 0$ to $\theta_{mag} = 54.74^\circ$, the local field field is reduced when

the form factor increases from -4 to 2 , between 54.74° and 125.26° the local field increases (Fig.2c). The strong dependence on the form factor is observed at small volumes, and this dependence decreases with increasing the cavity volume (Fig.2d). From experiments at $\theta = 0.96$, the spin-spin relaxation time T_2 was determined to be 1.3 ms [26]. The angle $\theta = 0.96$ is very close to the magic angle where the spin-spin relaxation due to DDI is relatively small, and one can observe the contribution of other mechanisms. The local field ω_{loc} is defined as $\frac{1}{T_2}$ [1, 32] which gives $\omega_{loc} \simeq 770$ Hz. Our estimation of the DDI contribution gives $\omega_{loc} \sim 400$ Hz. Therefore, the contribution of the non- DDI mechanisms to the local field can be estimated as ~ 370 Hz. With increasing deviation from the magic angle, the relative contribution of DDI to the local field increases.

During the time $T_2 \sim \omega_{loc}^{-1}$ the behavior of the spin system is described by the Hamiltonian H_{eff} , and a quasi-equilibrium state is established. Decrease of the magnetization during further evolution of the spin system is described by the time-dependent Hamiltonian part (22), $Q(t)$.

III. MULTIPLE PULSE SPIN LOCKING STATE AND STEADY-STATE MAGNETIZATION

The spin locking state can be achieved by a technique which provides the magnetization to be parallel to an effective field ω_e . A quite simple but convincing experiment, to reach the spin locking state, consists in the application of the first short RF $(\frac{\pi}{2})_y$ pulse that turns the magnetization along the x -axis. At high temperature approximation, the density matrix just after the $(\frac{\pi}{2})_y$ pulse is given by the following expression

$$\rho(0) = 1 - \alpha_0 \omega_0 I_x, \quad (24)$$

where α_0 is the initial inverse temperature of the Zeeman reservoir. Then the phase of the RF pulses is suddenly changed to zero, so that the RF field of multiple pulse sequence becomes directed along the x -axis, i.e. in the same direction as the magnetization.

The last terms in the effective dipolar Hamiltonian (21) contain flip-flop terms $I_i^+ I_j^- + I_i^- I_j^+$ [15], that ensures establishment of the quasi-equilibrium state of the spin system for the time of order of the spin-spin relaxation time $T_2 \propto \omega_{loc}^{-1}$. A spin system in the quasi-equilibrium state can be described by the density matrix which is similar to the matrix

considered at the study of processes in bulk solids [32]

$$\rho_{eq} = 1 - \alpha_e H_{eff} , \quad (25)$$

where α_e is the inverse temperature of the spin system in the quasi-equilibrium state. During the establishment of the state ($t \lesssim T_2$) we may also neglect absorption of energy by the system from external RF fields and apply the law of the energy conservation (similarly to bulk solids [32]), i.e. the conservation of energy $\langle H_{eff} \rangle$,

$$Tr(\rho(0) H_{eff}) = Tr(\rho_{eq} H_{eff}) \quad (26)$$

from which follows that

$$\frac{M_e}{M_0} = \left(1 + m (3 \cos^2 \theta - 1)^2 \right)^{-1} , \quad (27)$$

where

$$m = \frac{3}{16} (N - 1) \left(1 + 3 \left(\frac{\sin(2\varphi)}{2\varphi} \right)^2 \right) \left(\frac{\gamma^2 \hbar F(\varepsilon)}{2\omega_e V} \right)^2 , \quad (28)$$

M_e is the projection of the steady-state magnetization at $t \gtrsim T_2$ on the observation axis, and M_0 is the magnetization immediately after the $(\frac{\pi}{2})_y$ pulse application.

In multiple pulse experiments with bulk solid samples the period t_c is usually chosen such that $\varphi \simeq \omega_{loc} t_c < 1$ [24, 25]. Figure 3 gives the steady-state magnetization as a function of θ and φ (Fig. 3a); θ and N (Fig. 3b); φ and N (Fig. 3c); V and N (Fig. 3d); φ and V (Fig. 3e); θ and V (Fig. 3f).

The normalized magnetization M_e/M_0 is changed within from 10% up 40% with variation of the orientation of the nanocavity θ , the pulse duration t_c and the number of spins in the cavity N , and volume V at constant form factor, F (Fig. 3). Variations of θ and φ lead to the change of the normalized magnetization by about 30% with other parameters constant (Fig. 3a). The change of M_e/M_0 of the order of 10% is also obtained when the number of spins and the pulse duration are only varied (Figs. 3b and 3c). A significant change (up to 50%) in the magnetization is caused by varying the volume, especially, when the cavity volume is relatively small, about 10-25 nm³ (Figs. 3d, 3e, 3f). Change in magnetization with variation of the form factor is shown in Fig. 4: as a function of φ and F (Fig 4a); θ and F (Fig. 4b); V and F (Fig. 4c); N and F (Fig. 4d). It can be stated that the change in the magnetization varies from 50% (Figs. 4a, 4c) to 60% (Figs. 4b and 4d).

The results obtained above are valid for the case when all cavities in the sample have the same orientation (Fig. 1a). Such cavernous material, for example, was described in [26, 42]. To compare the experimental data and theoretical results in the case when the cavities are oriented arbitrarily, it is necessary to perform averaging of the steady-state magnetization over θ . At uniform distribution of directions over angle θ , the averaged normalized magnetization is:

$$\left\langle \frac{M_e}{M_0} \right\rangle_\theta = \frac{1}{2} \int_0^\pi d\theta \sin \theta \frac{M_e}{M_0}. \quad (29)$$

The integration gives

$$\left\langle \frac{M_e}{M_0} \right\rangle = \frac{\sqrt{3}}{6\sqrt{m}} \left(\frac{\arctan \frac{i\sqrt{3}}{\sqrt{1+i\frac{1}{\sqrt{m}}}}}{\sqrt{1+i\frac{1}{\sqrt{m}}}} - \frac{\arctan \frac{i\sqrt{3}}{\sqrt{1-i\frac{1}{\sqrt{m}}}}}{\sqrt{1-i\frac{1}{\sqrt{m}}}} \right). \quad (30)$$

Equation (30) can be converted to an expression containing only real variables, but this expression is too cumbersome and we do not give its explicit form here. Fig. 5 presents the averaged value of the steady-state magnetization as a function of φ and V (Fig. 5a); φ and N (Fig. 5b); φ and F (Fig. 5c); V and N (Fig. 5d).

In the case of disoriented cavities, the averaged normalized steady-state magnetization $\langle M_e/M_0 \rangle$ is changed within to 60% with variation of the pulse duration t_c , the number of spins in the cavity N and volume V at constant form factor F (Fig. 5). The largest change in the magnetization as a function of the form factor (Fig. 6) is achieved at large number of spins (Fig. 6a), low volumes (Fig. 6b) and small φ (Fig. 6c).

IV. EVOLUTION OF THE SPIN SYSTEM DURING MULTIPLE-PULSE SPIN LOCKING

After establishing the quasi-equilibrium state of a spin system, described by Eq. (25), further evolution of the spin system, at times $t \gg T_2$, is characterized by a slow change of the effective energy $\langle H_{eff} \rangle$. The change of the effective energy is governed by the time-dependent terms of the Hamiltonian (22). In the high temperature approximation, using the results for a bulk solid [46], we can write

$$\frac{d}{dt} \langle H_{eff} \rangle = -Tr (H_{eff}^2) \frac{d\alpha_e(t)}{dt} \quad (31)$$

The equation for the inverse temperature $\alpha_e(t)$ will be derived by using the method of the non-equilibrium state operator [46] which gives

$$\frac{d\alpha_e(t)}{dt} = -\frac{\alpha_e(t)}{T_{1e}}, \quad (32)$$

where T_{1e} is the characteristic time of the spin lattice relaxation during the multiple-pulse RF irradiation of the spin system

$$T_{1e} = \lim_{\xi \rightarrow 0} \frac{\text{Tr}(H_{eff}^2)}{\int_0^1 d\lambda \int_{-\infty}^0 dt e^{-\xi t} \langle [e^{(\lambda+it)H_{eff}} Q(t) e^{-(\lambda+it)H_{eff}}, H_{eff}] [H_{eff}, Q(t)] \rangle}, \quad (33)$$

where $\langle \dots \rangle$ notes the thermodynamic averaging with the quasi-equilibrium operator (25).

Using relation $\frac{M_e(t)}{M(T_2)} = \frac{\alpha_e(t)}{\alpha_e(T_2)}$, we obtain that the nuclear magnetization relaxes according to the expression

$$M_e(t) = M_e(T_2) e^{-\frac{t}{T_{1e}}}, \quad (34)$$

where $M_e(T_2)$ is the steady-state magnetization just after the establishment of the quasi-equilibrium state, considered as the initial value for the relaxation process.

To calculate the relaxation time T_{1e} , one has to know the correlation function $g_{qq}(t, t') = \langle Q(t)Q(t') \rangle$. Following [43], we will assume that the function $g_{qq}(t, t')$ depends on t and t' only through their differences $t - t'$. As in the case of a solid [43], we assume an exponential correlation function defined by

$$g_{qq}(t - t') = \langle Q^2(0) \rangle e^{-\frac{|t-t'|}{\tau_c}}. \quad (35)$$

Eq. (33) can be expressed as

$$T_{1e} = \frac{1}{W(3 \cos^2 \theta - 1)^2}, \quad (36)$$

where

$$W = t_c \frac{9}{2\zeta} \left(\frac{\gamma^2 \hbar}{2V} F(\varepsilon) \right)^2 (N - 1) \left(1 - \frac{1}{\zeta} \frac{(1 - \cos 2\varphi) \sinh \zeta}{\cosh \zeta - \cos 2\varphi} \right) \quad (37)$$

and $\zeta = \frac{2t_c}{\tau_c}$.

Expressions (36) and (37) give the dependence of the spin lattice relaxation time on the correlation time τ_c , period of the pulse sequence t_c , local magnetic field ω_e , the characteristics of gas or liquid inside the cavity: volume V , number of the molecules N , and parameters of the cavity: shape $F(\varepsilon)$ and orientation θ . Fig. 7 presents the obtained from (36) dependencies of $T_{1e}t_c$ on θ and φ (Fig. 7a), θ and ζ (Fig. 7b), V and N (Fig. 7c), V and ζ

(Fig. 7d). Figs. 7a and 7b show that the relaxation time increases sharply at orientations of the cavity close to $\theta_{mag} = 54.74^\circ$ and $\theta = 125.26^\circ$. At $\theta = 54.74^\circ$ and 125.26° , in the considered approximation, the averaged Hamiltonian terms (4) are zero and, for correct description of processes, one should consider next approximations. In experiments, parameter ζ can vary in the wide range from 0.01 to 100, however, the main peculiarities of the relaxation time on ζ lie near the point $\zeta = 1$ (Figs. 7b and 7d). At $\zeta \gg 1$, the relaxation time increases proportionally to this parameter, but does not exceed the value at $\zeta \ll 1$. The relaxation time T_{1e} decreases as ζ increases and attains its minimum at $\zeta \sim 1$. For a gas, the relaxation time increases with the cavity volume as V^2 and decreases with spin number as $\sim 1/N$ (Figs. 7c and 7d). It is interesting that for liquid, when the spin density is constant, the relaxation time is independent of the spin number and linearly increases with the cavity volume. Usually in experiments $t_c \simeq 10^{-5} s$ [24, 25] and from our results T_{1e} is estimated to be from 0.05 s up to 30 s (Fig. 7).

At uniform distribution of directions of the cavity axes over angle θ (Fig. 1a), to compare the experimental relaxation data and theoretical results, it is necessary to perform averaging of the magnetization over θ :

$$\langle M_e(t) \rangle_\theta = \frac{1}{2} \int_0^\pi d\theta \sin \theta M_e(T_2) e^{-\frac{t}{T_{1e}}} \quad (38)$$

The integral in (38) cannot be solved in quadratures, the results of the numerical calculation are shown in Figs 8 and 9. Fig. 8 presents the averaged normalized magnetization as a function of N and V (a) at $t = 5$ s and (b) $t = 50$ s. Figure 9 shows the time dependence of the normalized magnetization. This dependence is substantially non-exponential (Fig. 9b). In the initial stage of relaxation at $t \gg T_2$, the magnetization decays with the characteristic relaxation time $\langle T_{1e} \rangle_\theta \simeq 5$ s (Fig. 9c) while in the last stage the characteristic time is $\langle T_{1e} \rangle_\theta \simeq 286$ s (Fig. 9d). This can be explained by the following. The relaxation in the cavities oriented along and opposite the external magnetic field occurs faster than the relaxation in the cavities with the axes oriented near magic angles: $\theta = 54.74^\circ$ and 125.26° (Fig. 7). The value of the spin-lattice relaxation times $\langle T_{1e} \rangle_\theta$ well agree with those obtained in the case of continuous spin locking, while the time dependence of the magnetization is non-exponential [15].

V. CONCLUSION

Our study has shown that the spin locking state can be realized in gases and fluids confined in nanocavities. We have obtained analytical expressions that describe the dependence of the magnetization on the structural parameters of a nanocavity and the characteristics of a gas or a liquid. It was shown that the relaxation measurements can also be used to determine the volume and shape of a nanocavity, for both the ordered and disordered isotropic orientations of nanocavities. The theoretical models we considered in this work touch upon various soft matter and biological systems. This model can be used for the description the relaxation processes in liquid crystals and other anisotropic liquids under the condition that intramolecular dipole–dipole couplings are not averaged completely. The most obvious connection comes from the physics of molecules dissolved in complex fluids. Our approach can be used to characterize complex fluids confined on the nanoscale. Our results are also relevant in the situation when nanoconfining is provided by a vesicle, in particular, in biological systems. Finally, we would like to point out an advantage of the proposed multiple-pulse spin locking measurement method of the magnetization and relaxation time over the NMR cryoporometry technique [14, 44, 45]: the measurements of M_e (ordered) and $\langle M_e \rangle_\theta$ (isotropically disordered), along with the information about the cavity size, allow determining the shape and orientation of the cavity.

-
- [1] A. Abragam, *The Principles of Nuclear Magnetism*, Oxford Clarendon Press, 1961.
 - [2] C.P. Slichter, *Principles of Magnetic Resonance* (Springer Series in Solid-State Sciences), 1996.
 - [3] P. G. de Gennes and J. Prost, *The Physics of Liquid Crystals*, Oxford Clarendon Press, 1995.
 - [4] P. T. Callaghan, *Principles of Nuclear Magnetic Resonance Microscopy*, Oxford Clarendon Press, 1991.
 - [5] E. Breitmaier, *Structure Elucidation by NMR in Organic Chemistry: A Practical Guide*, John Wiley&Sons Ltd., 2002
 - [6] C. Alba-Simionesco, B. Coasne, G. Dosseh, G. Dudziak, K. E. Gubbins, R. Radhakrishnan and M. Sliwinska-Bartkowiak, *J. Phys.: Condens. Matter* **18** R15 (2006).
 - [7] J.H. Strange and M. Rahman, *Phys. Rev. Lett.*, **71**, 3589 (1993).
 - [8] W.S. Warren, W. Richter, A.H. Andreotti, and B.T. Farmer II, *Science*, **262**, 2005 (1993)

- [9] W. Richter, S. Lee, W. S. Warren, and Q. He, *Science* **267**, 654 (1995).
- [10] R. Bowtell and P. Robyr, *Phys. Rev. Lett.* **76**, 497, (1996).
- [11] P. Robyr and R. Bowtell, *J. Chem. Phys.* **106**, **8**, 467, (1997).
- [12] P. Robyr and R. Bowtell, *J. Chem. Phys.*, **107**, 702 (1997).
- [13] R. Bowtell, S. Gutteridge and C. Ramanathan, *J. Magn. Reson.*, **150**, 147 (2001).
- [14] S.-Y. Ryu, D. S. Kim, J.-D. Jeon, and S.-Y. Kwak, *J. Phys. Chem. C* **114**, 17440 (2010).
- [15] E. B. Fel'dman, G. B. Furman, and S. D. Goren, *Soft Matter*, **8**, 9200, 2012.
- [16] G. Furman and S. Goren, *Z. Naturforsch.* **66a**, 779 (2011).
- [17] G. Furman and S. Goren, *Materials Science Forum*, **721**, 47 (2012).
- [18] E. B. Fel'dman, A. I. Zenchuk, *Chem. Phys.* **390**, 20, 2011
- [19] S. I. Doronin, E. B. Fel'dman, A. I. Zenchuk, *JETP*, **113**, 495 (2011).
- [20] G. B. Furman and S D Goren, *J. Phys.: Condens. Matter* **17**, 4501, 2005.
- [21] S.D. Doronin, E.B. Fel'dman, E.I. Kuznetsova, G.B. Furman, and S.D. Goren, *JETP Letters* **86**, 26, 2007.
- [22] S. I. Doronin, E. B Fel'dman, E. I. Kuznetsova, G. B. Furman, S.D. Goren, *Phys. Rev. B* **76**, 144405-1-5, 2007.
- [23] A.M. Panich and G.B. Furman, *Diamond and Related Materials*, **23**, 157 (2012).
- [24] U. Haebleren, *High resolution NMR in solids*, Academic Press, New York, 1976.
- [25] M. Mehring, *Principles of High Resolution NMR in Solids*, Springer-Verlag, New York, 1983.
- [26] J. Baugh, A. Kleinhammes, D. Han, Q. Wang, Y. Wu, *Confinement Effect on Dipole-Dipole Interactions in Nanofluids*, *Science*, **294**, 1505 (2001).
- [27] W. Richter, W. S. Warren, *Concepts Magn. Reson.*, **12**, 396 (2000).
- [28] M.G. Rudavets, E.B. Fel'dman, *JETP Letters*, **75**, 635-637 (2002).
- [29] E. B. Fel'dman and M. G. Rudavets, *JETP*, **98**, 207 (2004).
- [30] S. I. Doronin, A. V. Fedorova, E. B. Fel'dman, and A. I. Zenchuk, *J. Chem. Phys.* **131**, 104109 (2009).
- [31] T. Tsukahara, W. Mizutani, K. Mawatari, and T. Kitamori, *J. Phys. Chem. B* **113**, 10808 (2009).
- [32] Goldman M *Spin Temperature and Nuclear Resonance in Solids*, Oxford Clarendon Press, 1970.
- [33] D. K. Green and J. G. Powles, *Proc. Phys. Soc.*, **85**, 87 (1965).

- [34] J. Jeener, J. Chem. Phys., **112**, 5091(2000).
- [35] J. Jeener, J. Chem. Phys. **134**, 114519 (2011).
- [36] T. Gabler, A. Paschke, and G.Schuurmann, J. Chem. Eng. Data **41**, 33 (1996).
- [37] M. Holz, S.R. Heil, A. Sacco, Phys. Chem. Chem. Phys. **2**, 4740 (2000).
- [38] Yu. N. Ivanov, B. N. Provotorov, and E. B. Fel'dman, Pis'ma Zh. Eksp. Teor. Fiz. **27**, 164 (1978) (JETP Lett. **3**, 153 (1978)).
- [39] E. B. Fel'dman, Phys. Lett. 104A, 479 (1984).
- [40] M.Yu. Svetlov and G.B. Furman, Izv. Vuz. Radiof., **30**, 557 (1987).
- [41] Y. J. Chabal and C. K. N. Patel, Molecular hydrogen in a-Si:H, Reviews of Modern Physics, **59**, 835 (1987).
- [42] Y. Zhang, A. Faraone, W. A. Kamitakahara, K.-H. Liu, C.-Y. Mou, J. B. Leão, S. Chang, S.-H. Chen, Unusual phase behavior of nano-confined water: new insights. <http://arxiv.org/abs/1005.5387>
- [43] D. E. Woessner and H. S. Gutovsky, J. Chem. Phys. **39**, 440 (1963).
- [44] J. H. Strange, M. Rahman, E.C.Smith, Phys. Rev. Lett., **71**, 3589 (1993).
- [45] J. Mitchell, J. B. W. Webber, J.H. Strange, Physics Reports, **461**, 1 (2008).
- [46] D. N. Zubarev, Nonequilibrium Statistical Thermodynamics (Imprint Consultants Bureau, New York, 1974).

Caption figures

Fig. 1 Oriented (a) and disoriented (b) nanocavities containing water molecules (c). θ is the angle between the external magnetic field ($\vec{H}_0 \parallel \vec{z}$) and the principal axis a of the nanocavity.

Fig. 2 Local dipolar field (ω_{loc}) as a function of: (a) angle θ and volume V (nm^3) at $N=500$ and $F=2$, (b) angle θ and number of spins N in cavity at $V=20 \text{ nm}^3$ and $F=2$, (c) angle θ and form factor F at $V=20 \text{ nm}^3$ and $N=500$, (d) volume V and form factor F at $\theta=0$ and $N=500$.

Fig. 3 Normalized steady-state magnetization as a function of: (a) angle θ and φ at $V=50 \text{ nm}^3$, $N=500$ and $F=2$, (b) angle θ and number of spins N at $V=50 \text{ nm}^3$, $\varphi=\pi/2$ and $F=2$, (c) φ and N at $V=50 \text{ nm}^3$, $\theta=0$ and $F=2$, (d) volume V and number of spins N at $\varphi=\pi/2$, $\theta=0$ and $F=2$, (e) φ and V at $N=500$, $\theta=\pi/2$ and $F=2$, (f) θ and V at $N=500$, $\varphi=\pi/2$ and $F=2$. Here and in the figures below $\omega_e=1000 \text{ G}$.

Fig.4 Normalized steady-state magnetization as a function of: (a) φ and form factor F for $V=20 \text{ nm}^3$, $N=500$ and $\theta = \pi/2$, (b) θ and F at $V=20 \text{ nm}^3$, $\varphi = \pi/2$ and $N=500$, (c) V and F at $\theta = \pi/2$, $\varphi = \pi/2$ and $N=500$, (d) N and F at $\varphi = \pi/2$, $\theta = \pi/2$ and $V=20 \text{ nm}^3$.

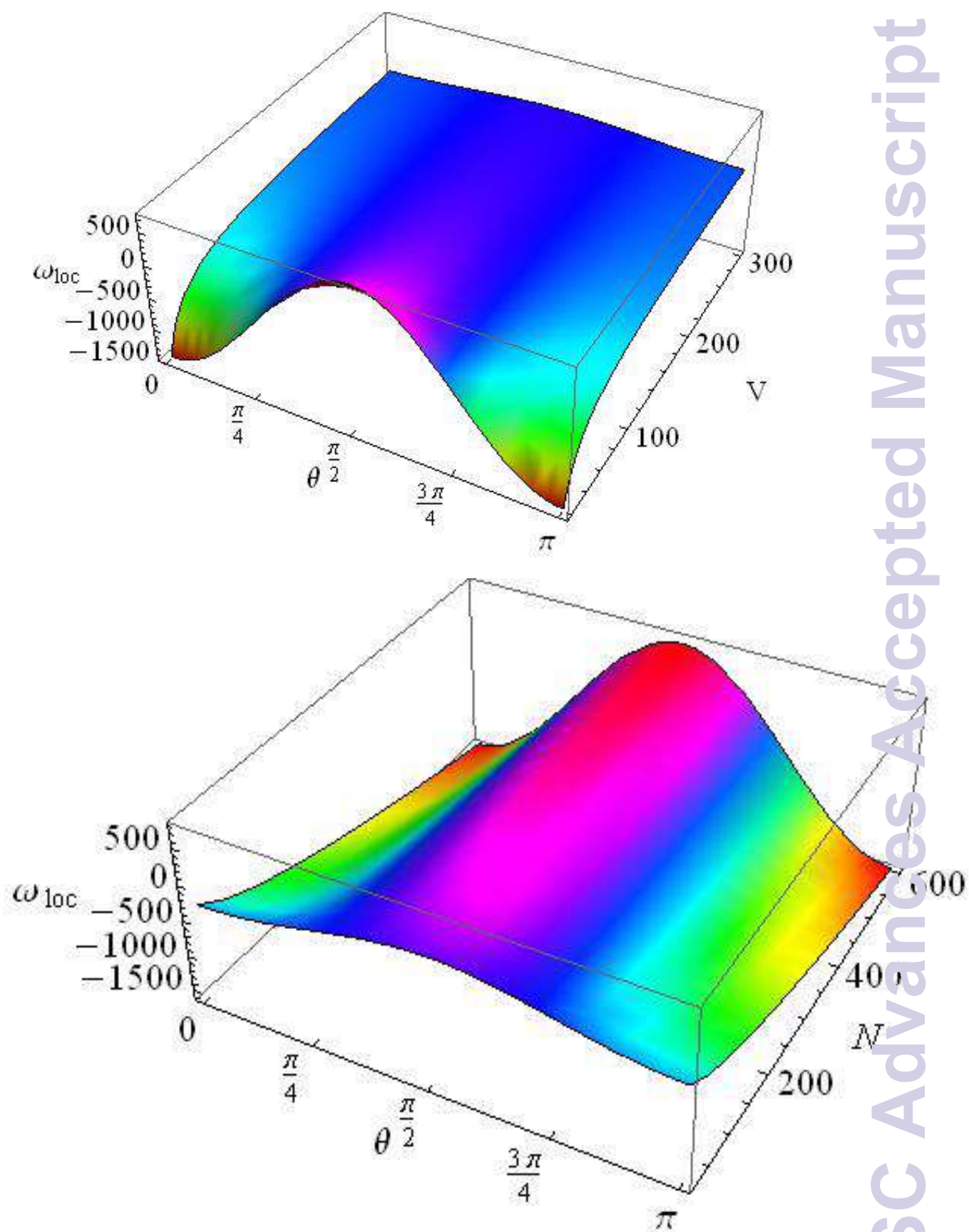
Fig. 5 Averaged normalized steady-state magnetization as a function of: (a) φ and V at $N=500$ and $F=2$, (b) φ and N at $V=20 \text{ nm}^3$ and $F=2$, (c) V and N at $\varphi = \pi/2$ and $F=2$.

Fig. 6 Averaged normalized steady-state magnetization as a function of: (a) N and F (a, $\varphi = \pi/2$, $V=20 \text{ nm}^3$); V and F (b, $N=500$, $\varphi = \pi/2$); φ and F (c, $V=20 \text{ nm}^3$, $N=500$).

Fig. 7 $T_{1e}t_c$ as a function of: (a) θ and φ at $V=50 \text{ nm}^3$, $N=500$, $F=2$ and $\zeta=1$, (b) θ and ζ at $V=50 \text{ nm}^3$, $N=500$, $F=2$ and $\varphi = \pi/2$, (c) V and N at $\theta = 0$, $F=2$, $\varphi = \pi/2$ and $\zeta=1$, (d) V and ζ at $\theta = 0$, $F=2$, $\varphi = \pi/2$, $\zeta=1$ and $N=500$.

Fig. 8 Averaged normalized magnetization as a function of N and V : (a) $t = 5 \text{ s}$, (b) $t = 50 \text{ s}$ ($F = 2$, $\varphi = \pi/2$, $\zeta = 1$, $t_c = 10^{-5} \text{ s}$).

Fig. 9 Time dependence of the averaged normalized magnetization (a) and of $\ln \langle \frac{M_e}{M_0} \rangle$ (b). (c) and (d) demonstrate different time constants of the dependence of $\ln \langle \frac{M_e}{M_0} \rangle$ in different stages of the relaxation: (c) $0 < t < 2 \text{ s}$ and (d) $50 \text{ s} < t < 100 \text{ s}$. Here $N=500$, $V=50 \text{ nm}^3$, $F=2$, $\varphi = \pi/2$, $\zeta=1$, $t_c=10^{-5} \text{ s}$.



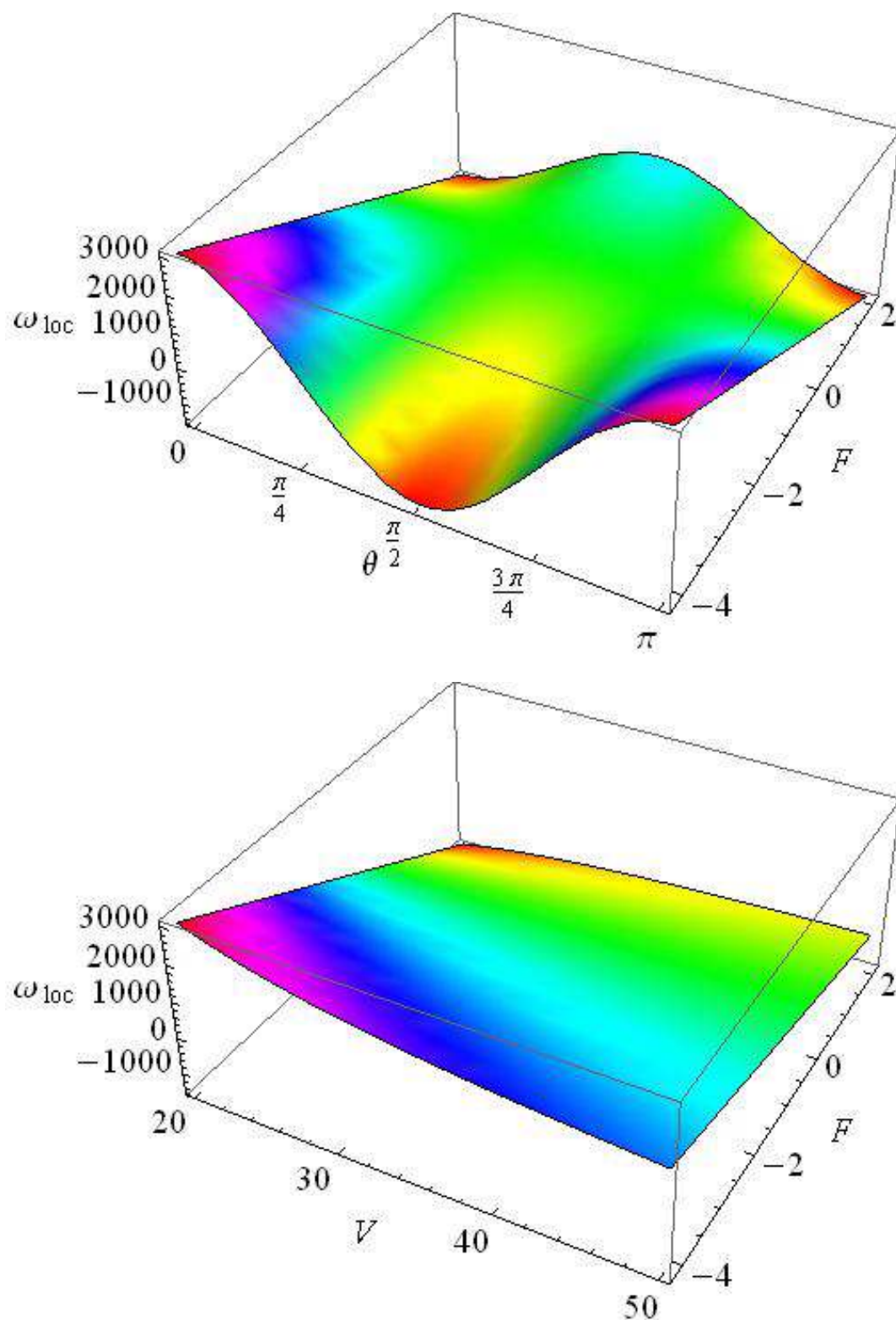
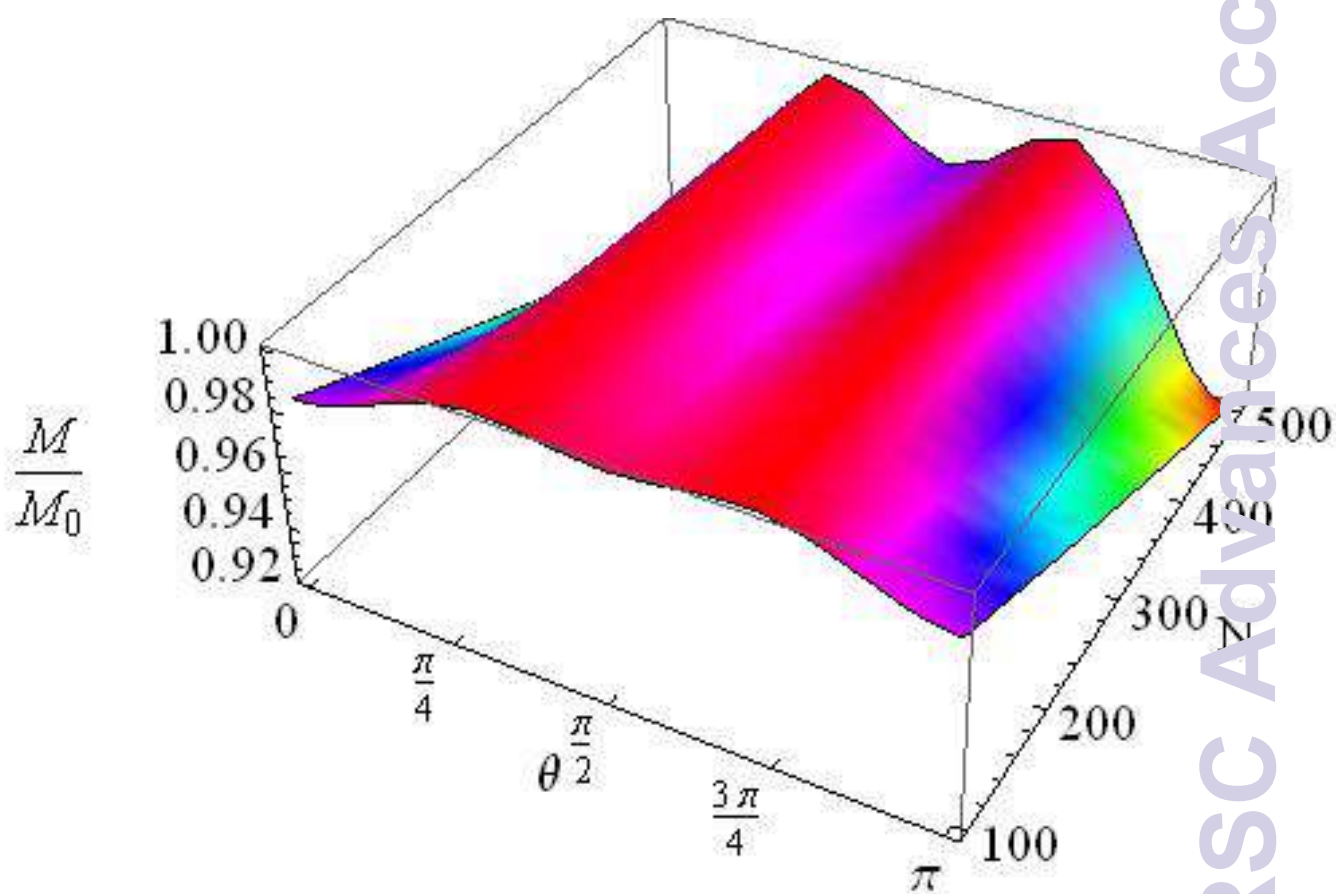
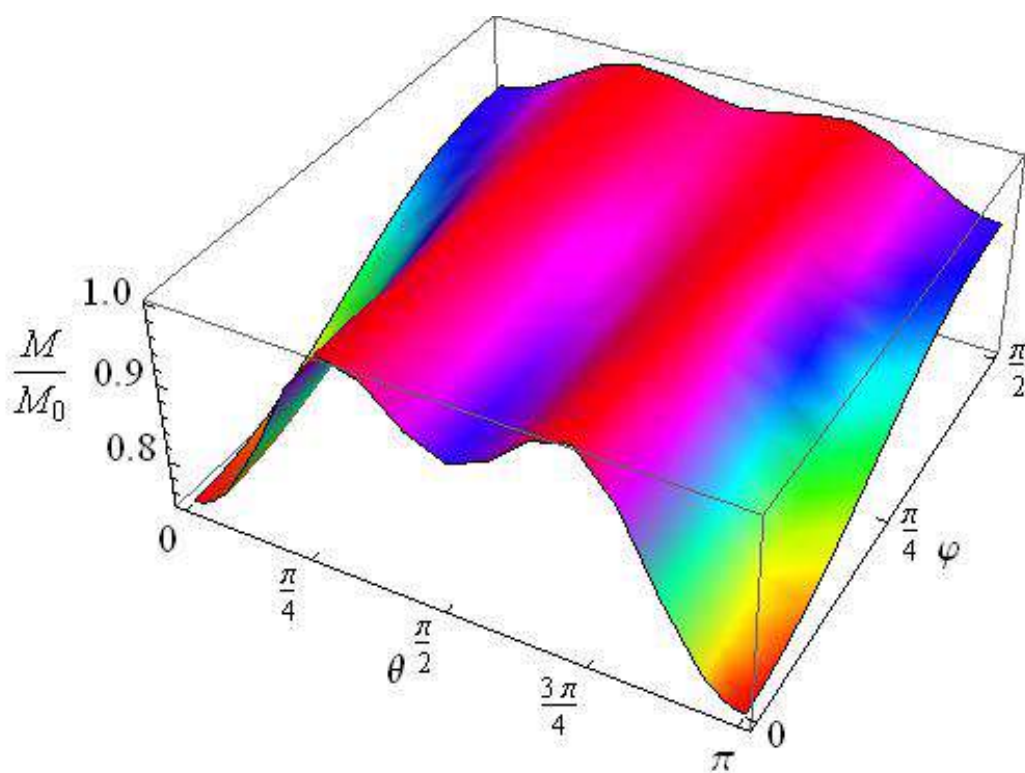
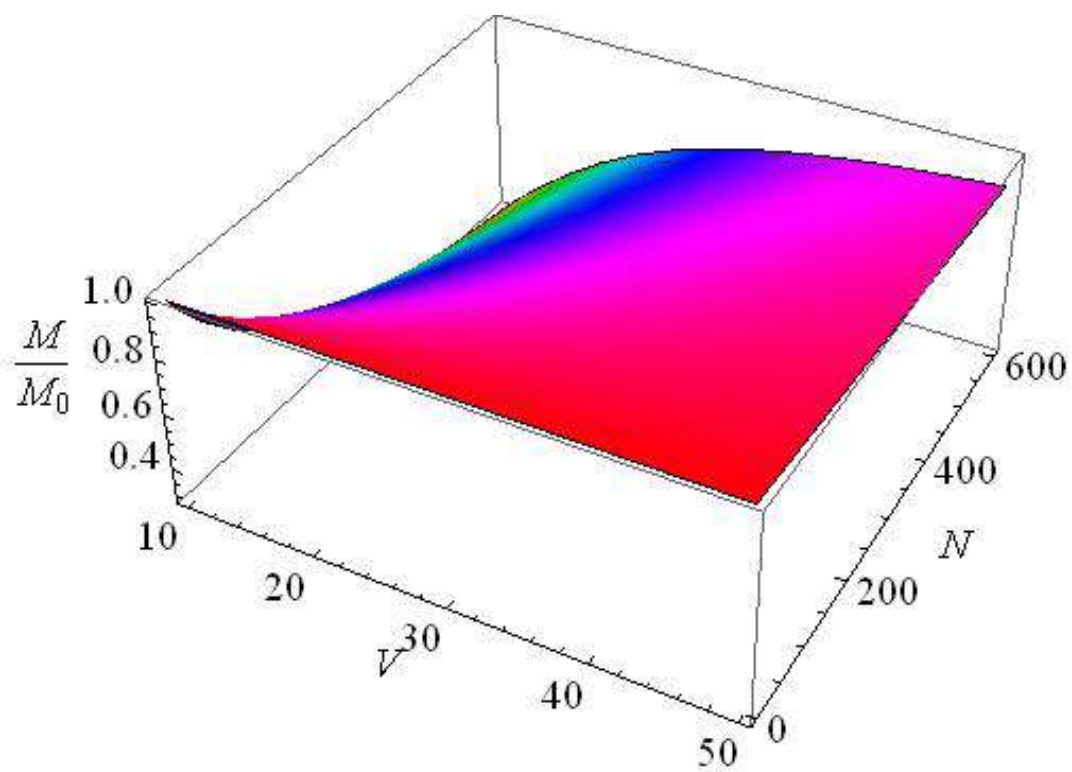
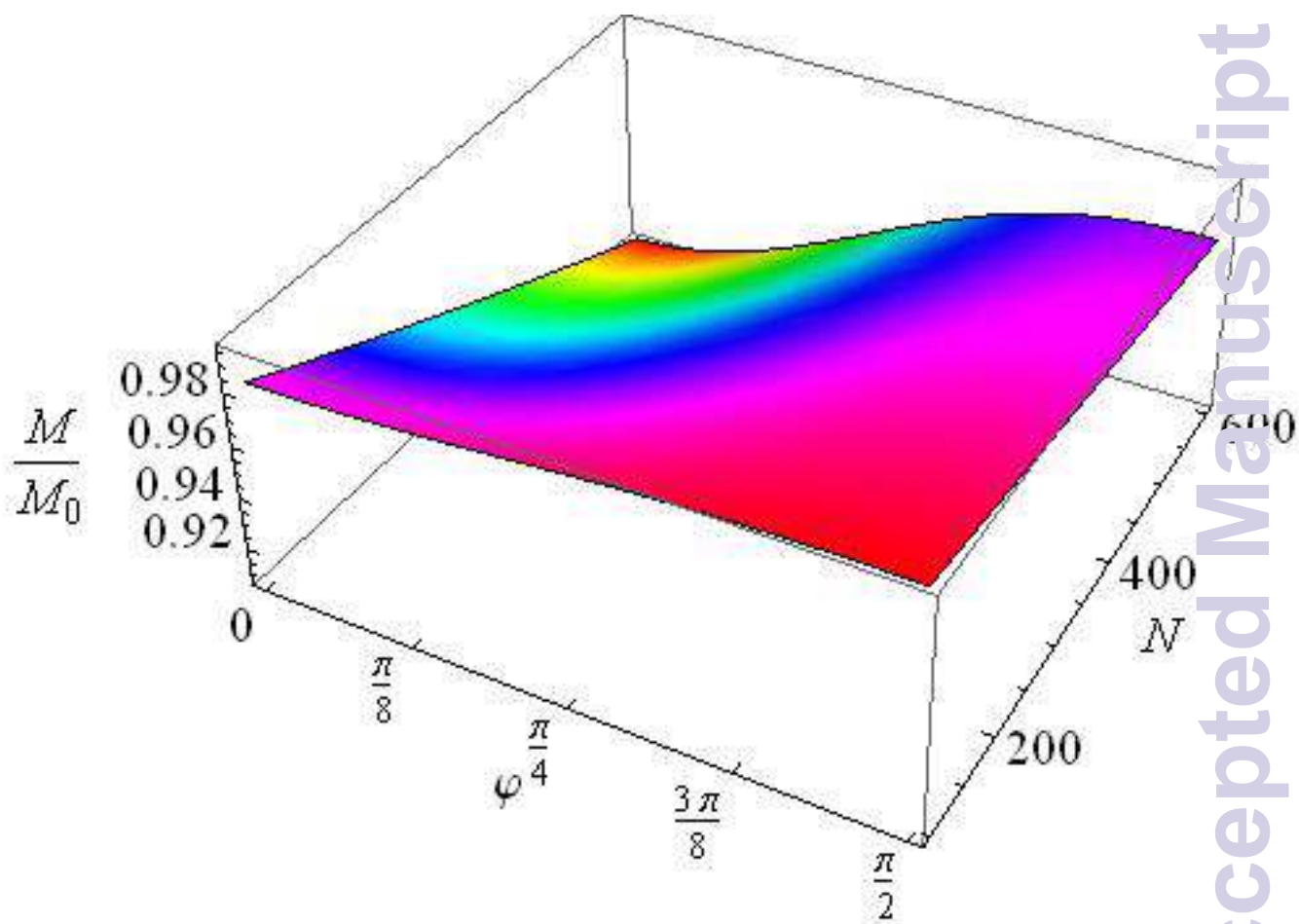


Fig. 2 Local dipolar field (ω_{loc}) as a function of: (a) angle θ and volume V (nm^3) at $N=500$ and $F=2$, (b) angle θ and number of spins N in cavity at $V=20 \text{ nm}^3$ and $F=2$, (c) angle θ and form factor F at $V=20 \text{ nm}^3$ and $N=500$, (d) volume V and form factor F at $\theta=0$ and $N=500$.

Fig. 3 Normalized steady-state magnetization as a function of: (a) angle θ and φ at $V=50 \text{ nm}^3$, $N=500$ and $F=2$, (b) angle θ and number of spins N at $V=50 \text{ nm}^3$, $\varphi=\pi/2$ and $F=2$, (c) φ and N at $V=50 \text{ nm}^3$, $\theta=0$ and $F=2$, (d) volume V and number of spins N at $\varphi=\pi/2$, $\theta=0$ and $F=2$, (e) φ and V at $N=500$, $\theta=\pi/2$ and $F=2$, (f) θ and V at $N=500$, $\varphi=\pi/2$ and $F=2$. Here and in the figures

below $\omega_e=1000$ G.





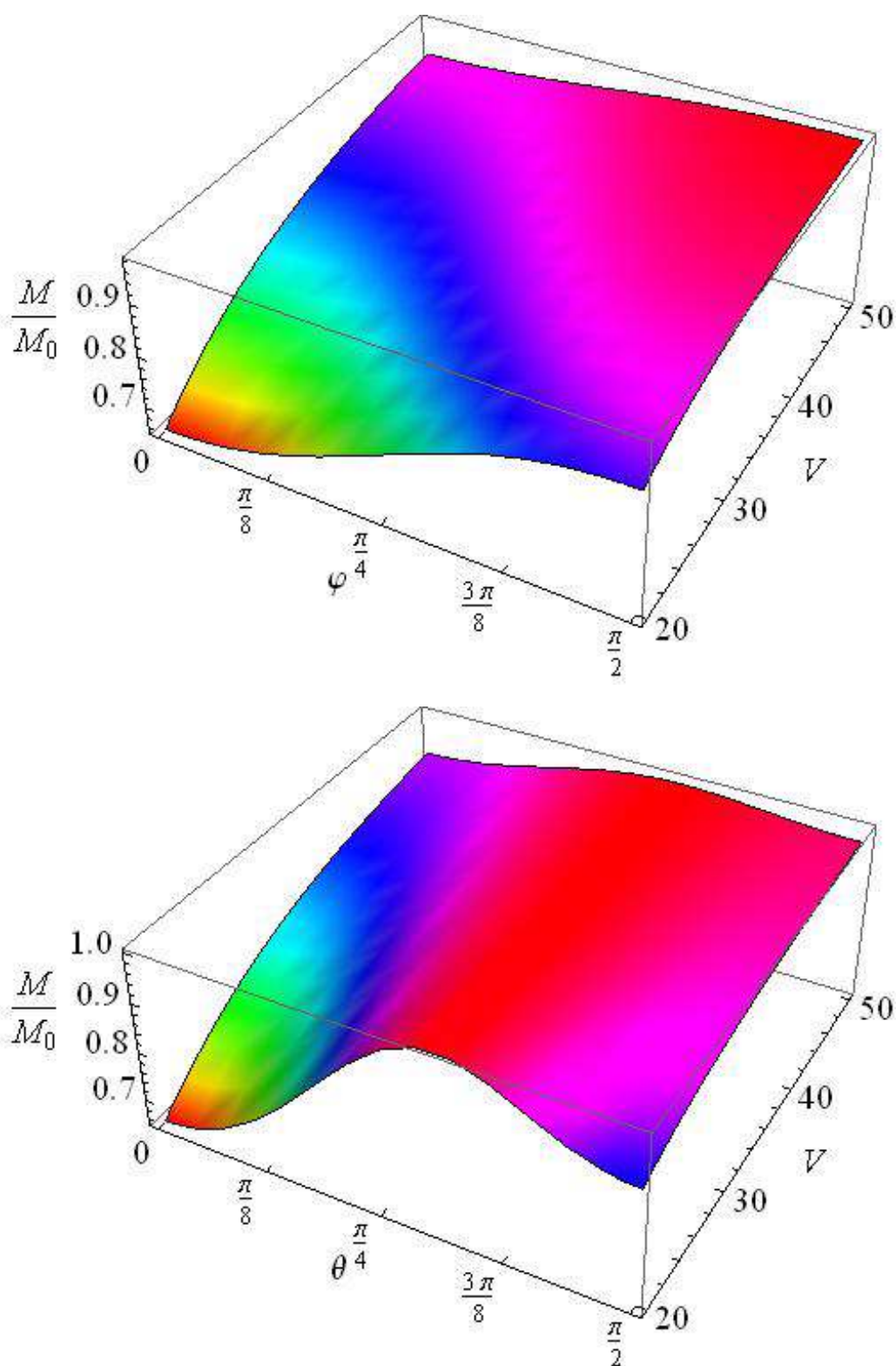
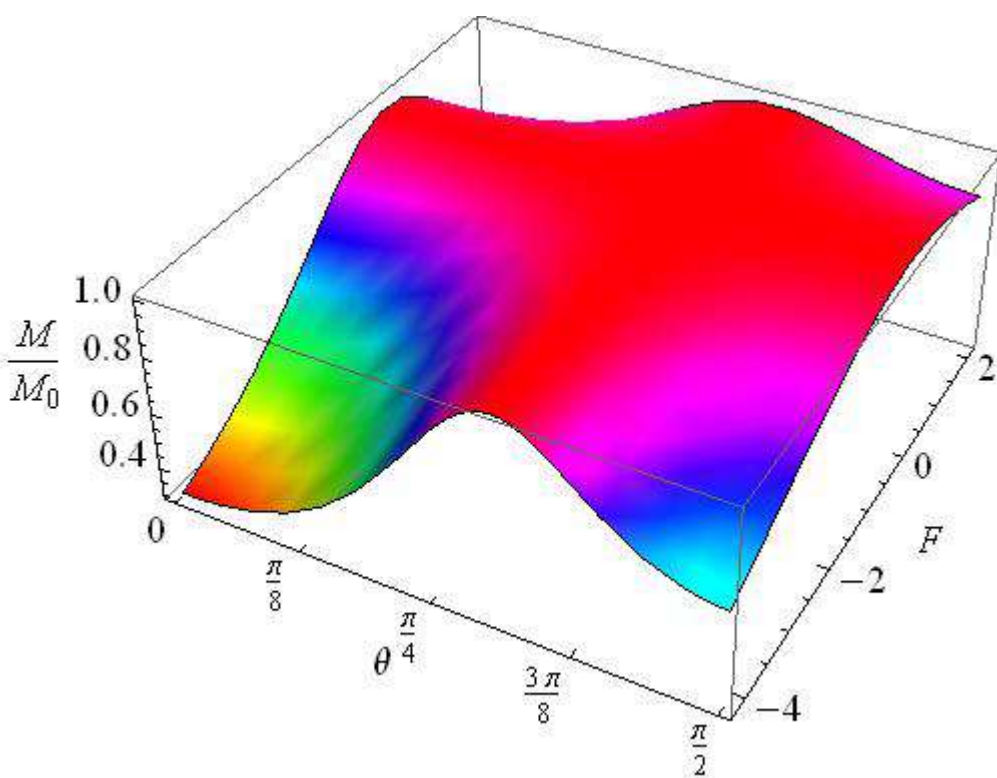
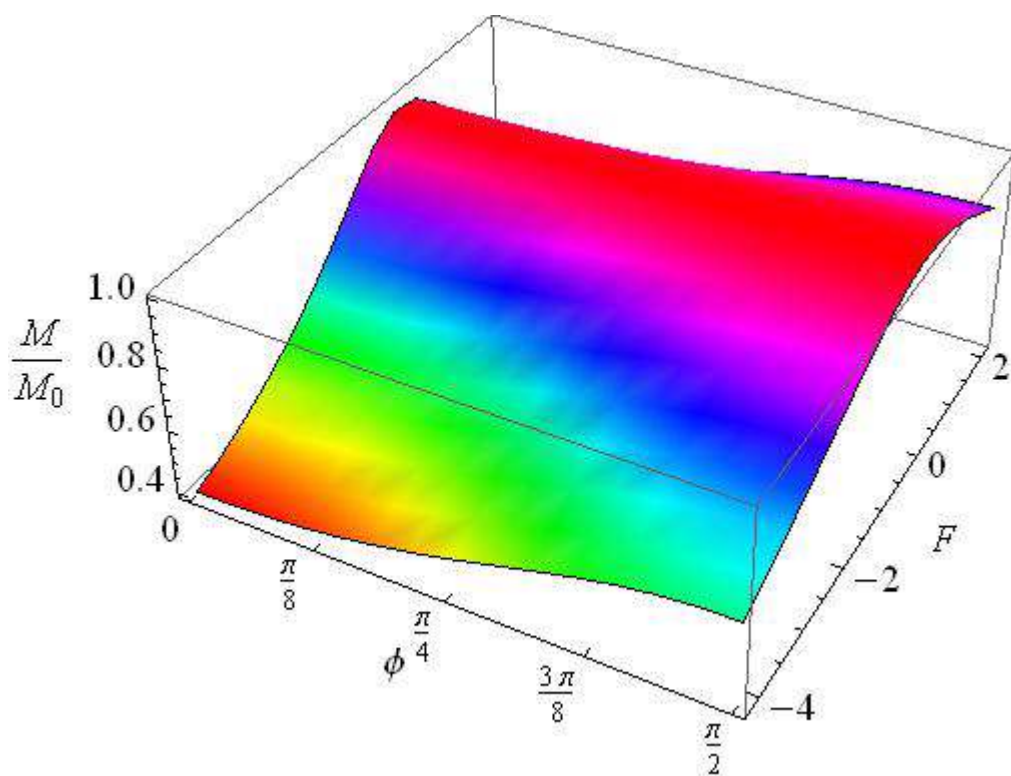
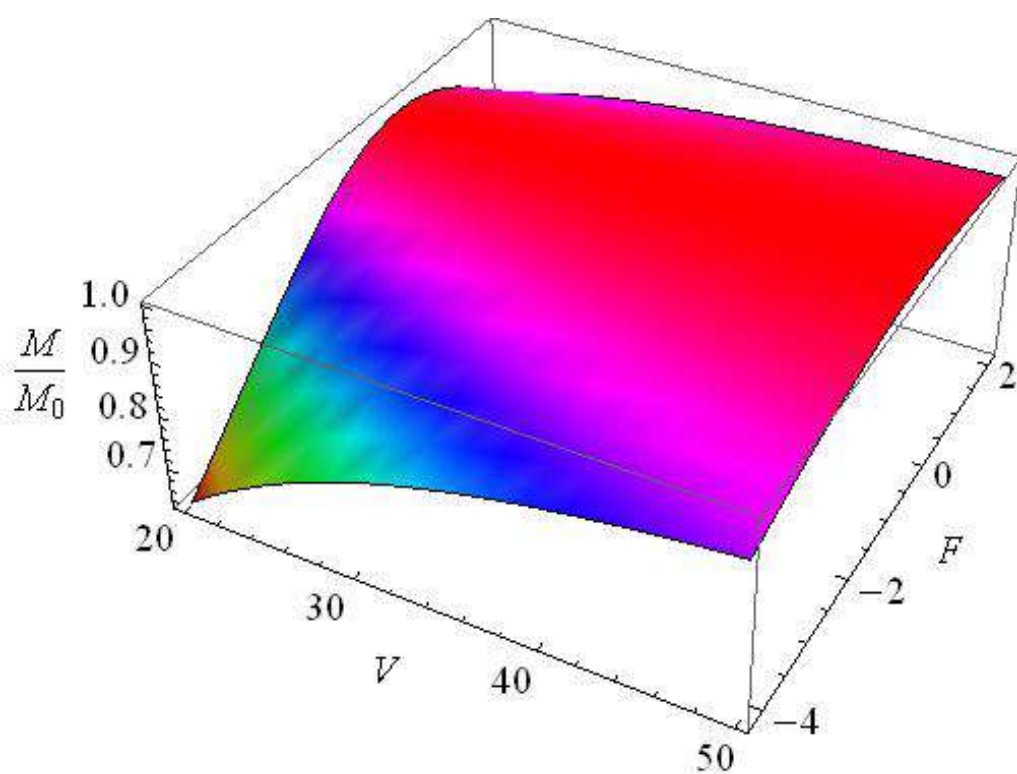
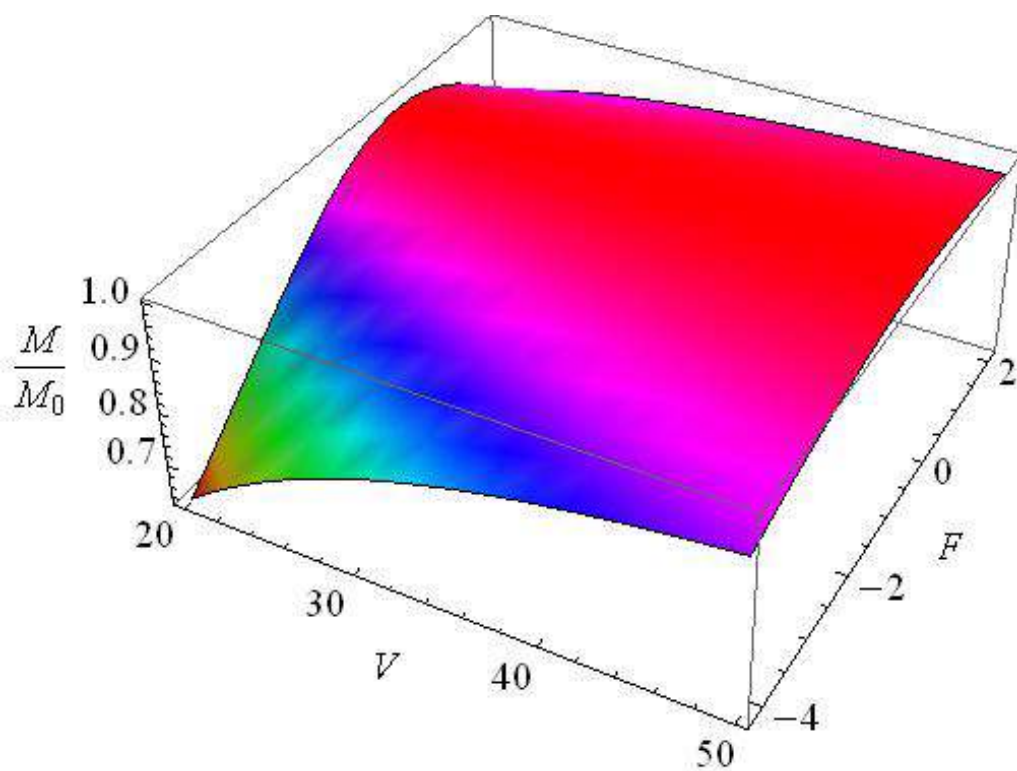


Fig.4 Normalized steady-state magnetization as a function of: (a) ϕ and form factor F for $V=20 \text{ nm}^3$, $N=500$ and $\theta = \pi/2$, (b) θ and F at $V=20 \text{ nm}^3$, $\phi = \pi/2$ and $N=500$, (c) V and F at $\theta = \pi/2$, $\phi = \pi/2$ and $N=500$, (d) N and F at $\phi = \pi/2$, $\theta = \pi/2$ and $V=20 \text{ nm}^3$.





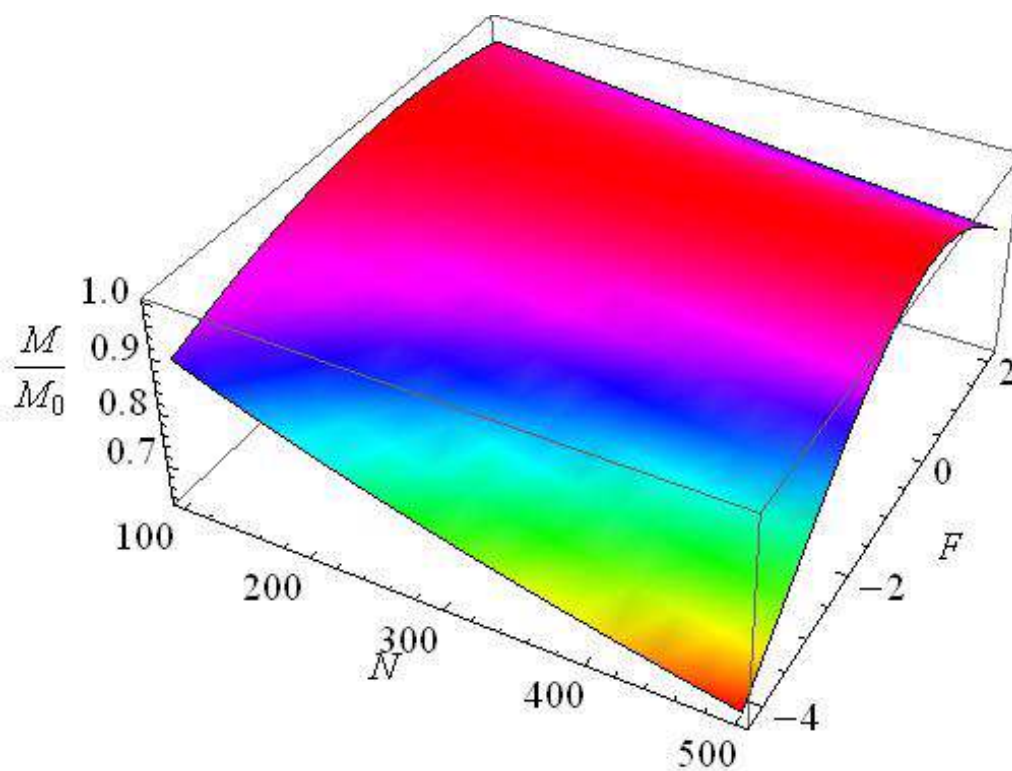
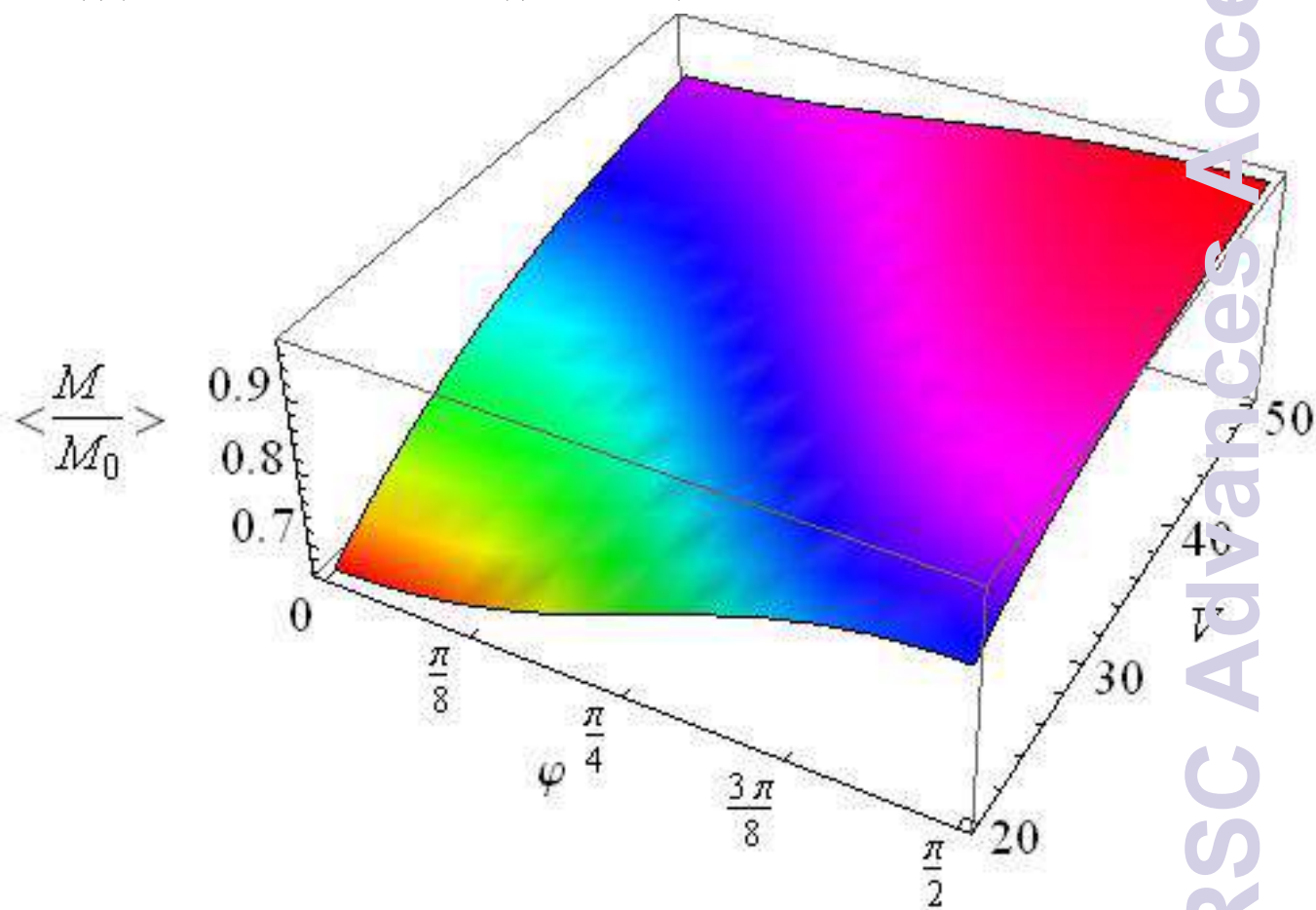


Fig. 5 Averaged normalized steady-state magnetization as a function of: (a) φ and V at $N=500$ and $F=2$, (b) φ and N at $V=20 \text{ nm}^3$ and $F=2$, (c) V and N at $\varphi=\pi/2$ and $F=2$.



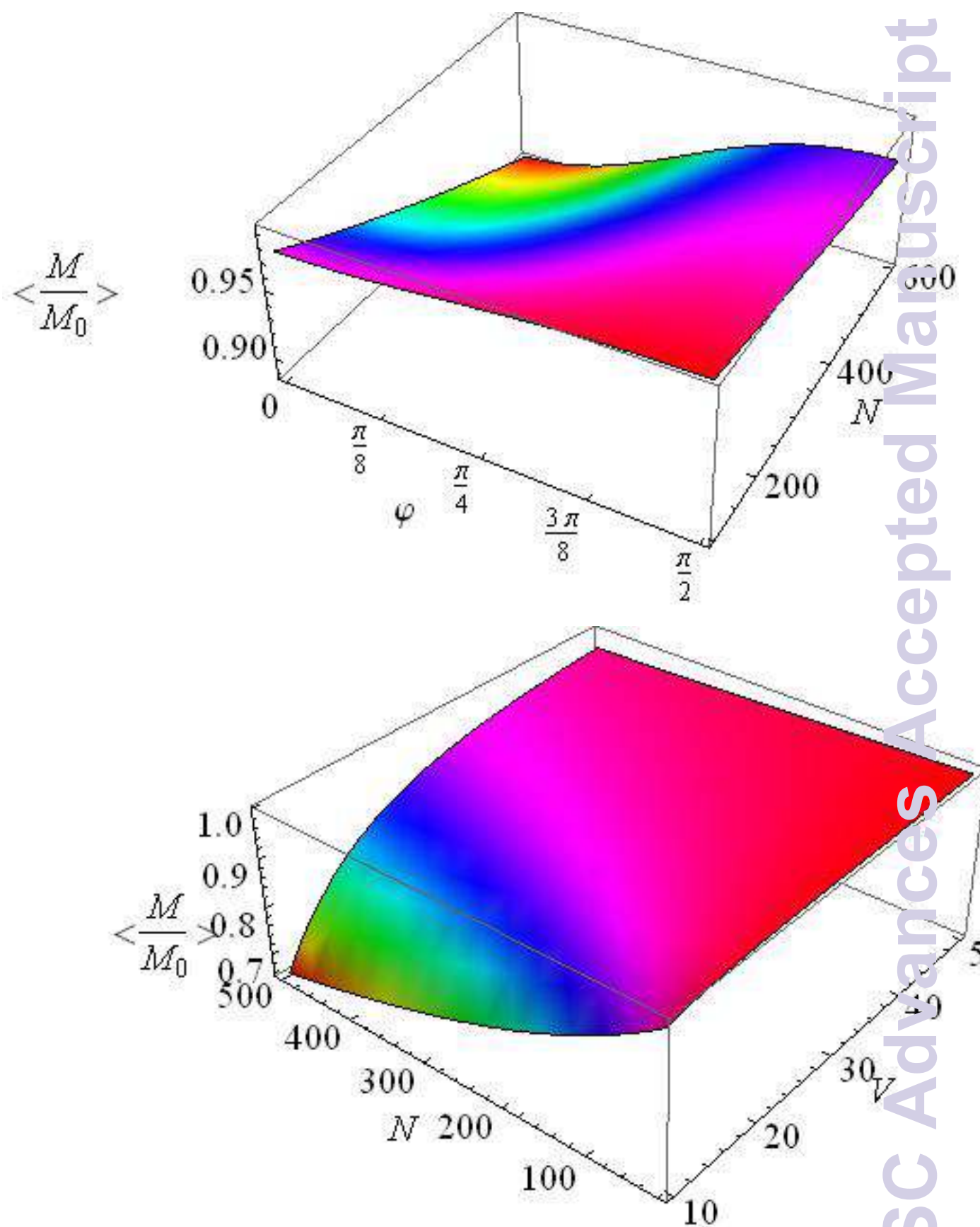
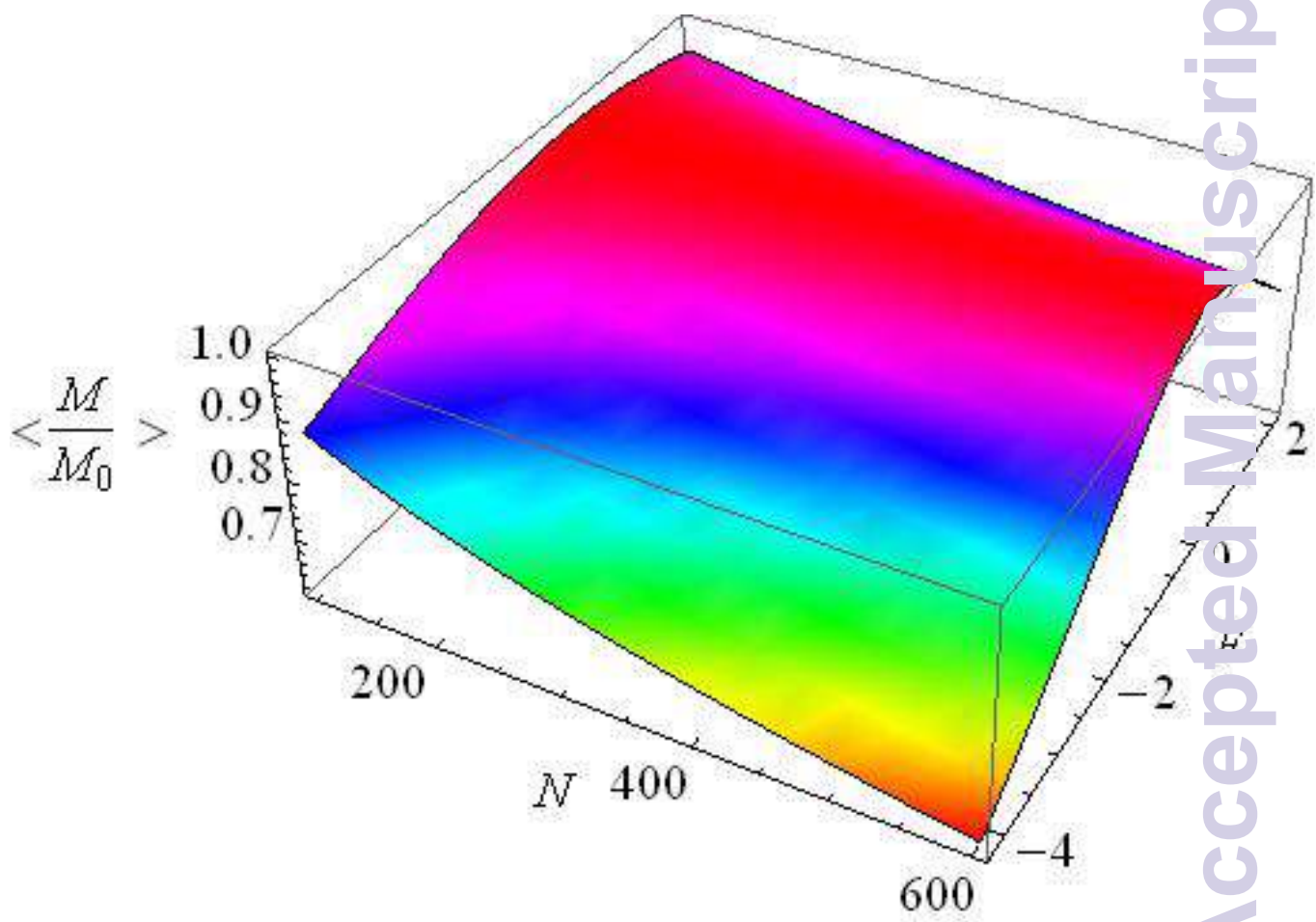


Fig. 6 Averaged normalized steady-state magnetization as a function of: (a) N and F (a, $\varphi = \pi/2$, $V = 20 \text{ nm}^3$); V and F (b, $N = 500$, $\varphi = \pi/2$); φ and F (c, $V = 20 \text{ nm}^3$, $N = 500$).



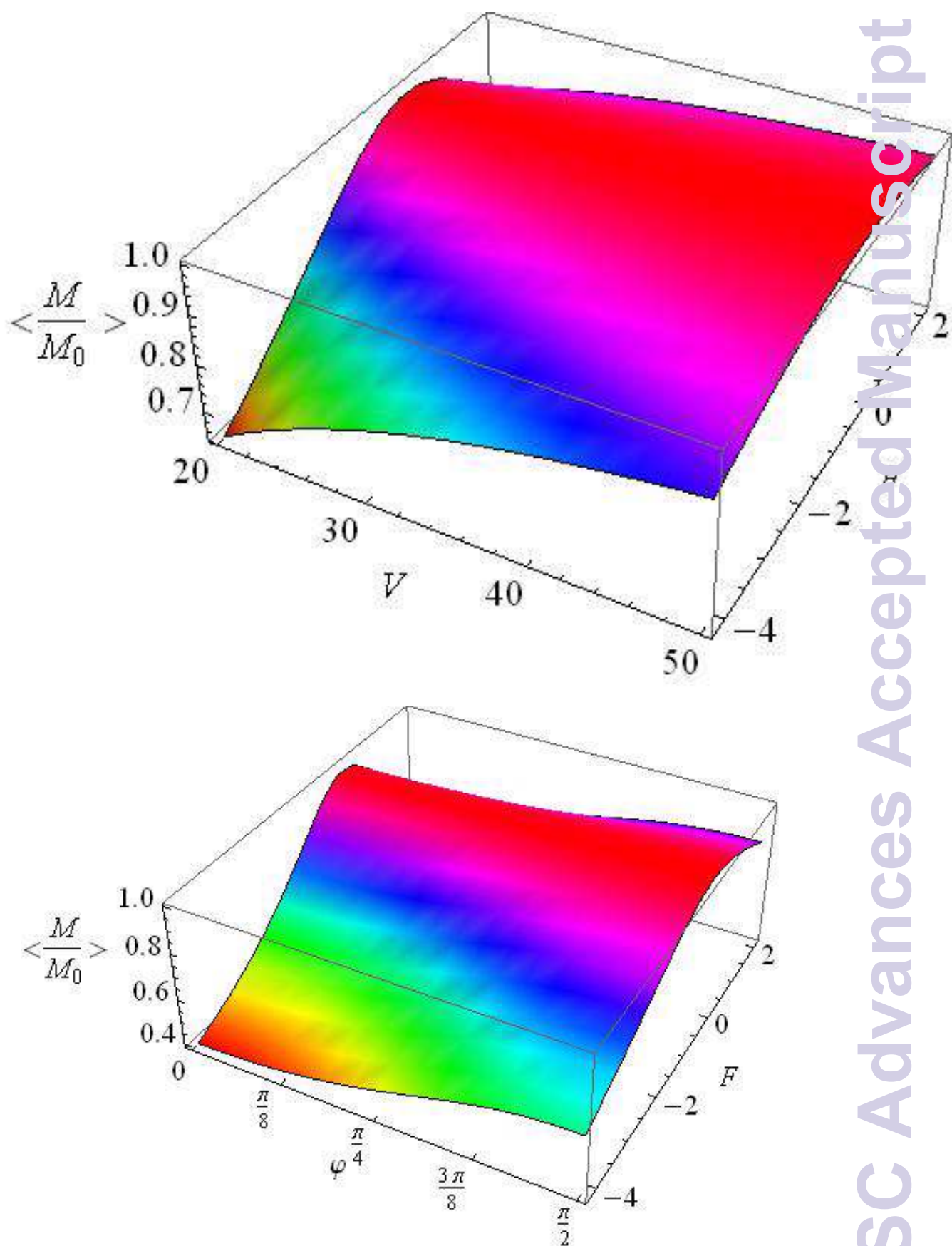
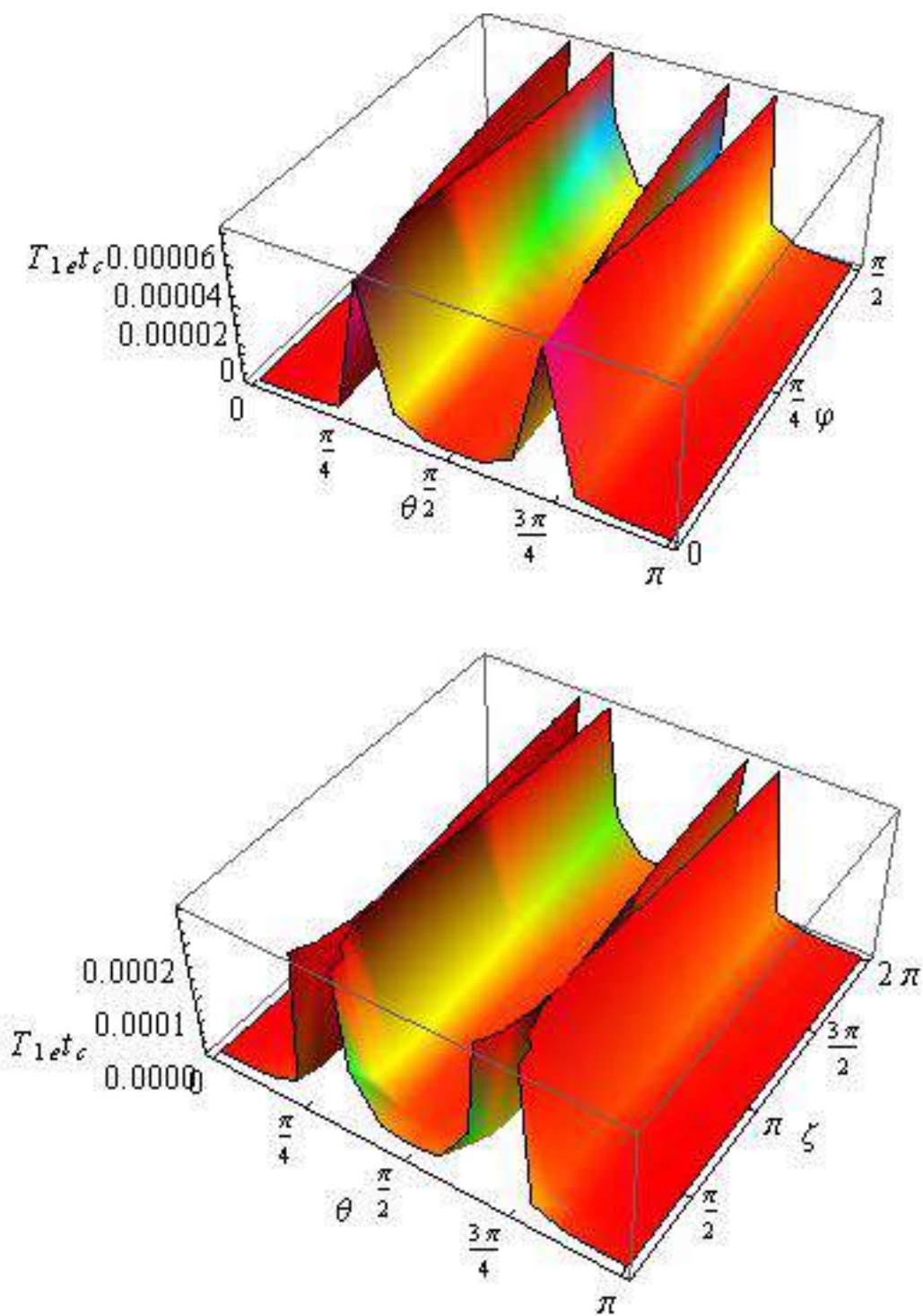


Fig. 7 T_{1c} as a function of: (a) θ and φ at $V=50 \text{ nm}^3$, $N=500$, $F=2$ and $\zeta=1$, (b) θ and ζ at

$V=50 \text{ nm}^3$, $N=500$, $F=2$ and $\varphi=\pi/2$, (c) V and N at $\theta=0$, $F=2$, $\varphi=\pi/2$ and $\zeta=1$, (d) V and ζ at $\theta=0$, $F=2$, $\varphi=\pi/2$, $\zeta=1$ and $N=500$.



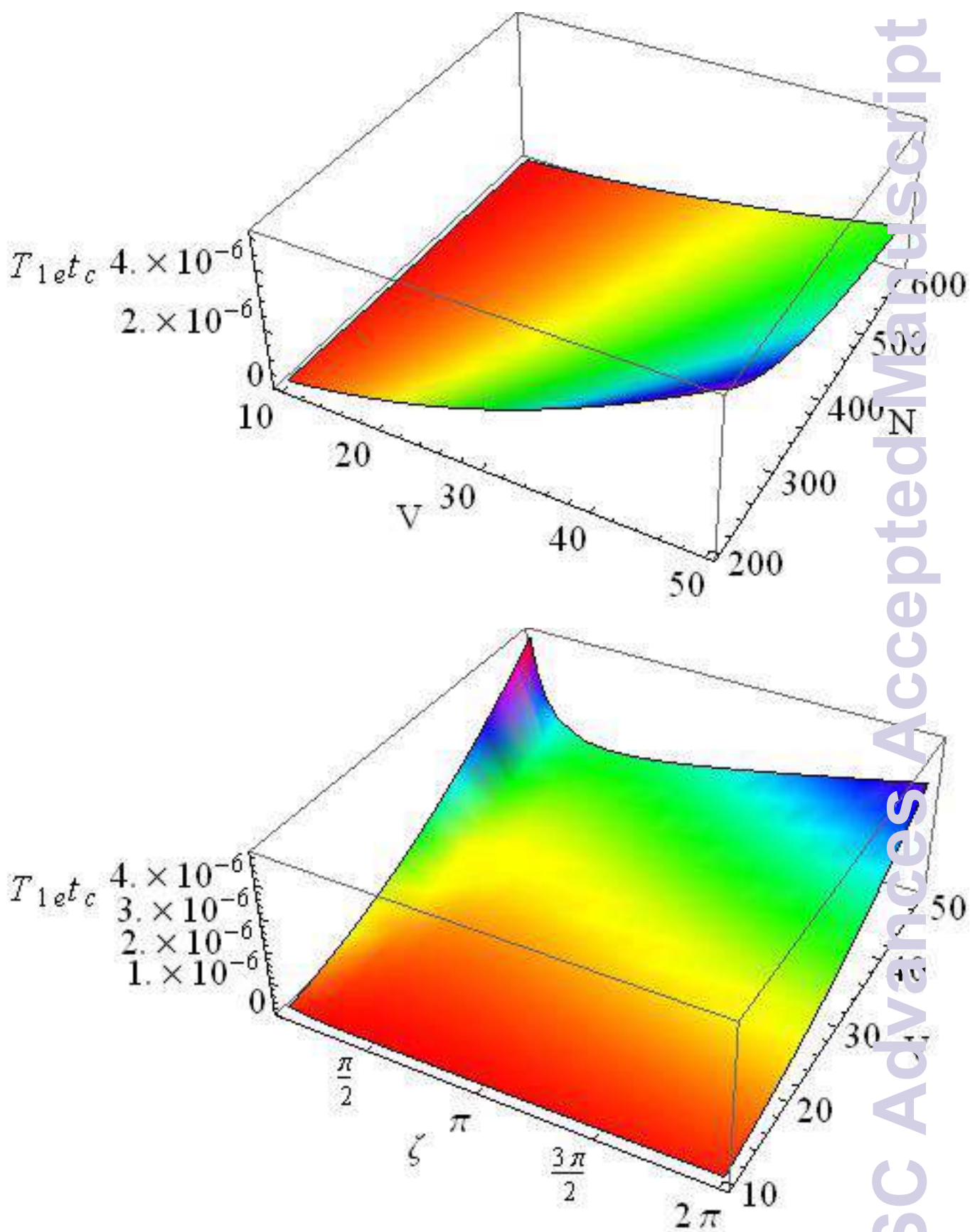


Fig. 8 Averaged normalized magnetization as a function of N and V : (a) $t=5$ s, (b) $t=50$ s ($F=2$, $\varphi=\pi/2$, $\zeta=1$, $t_c=10^{-5}$ s).

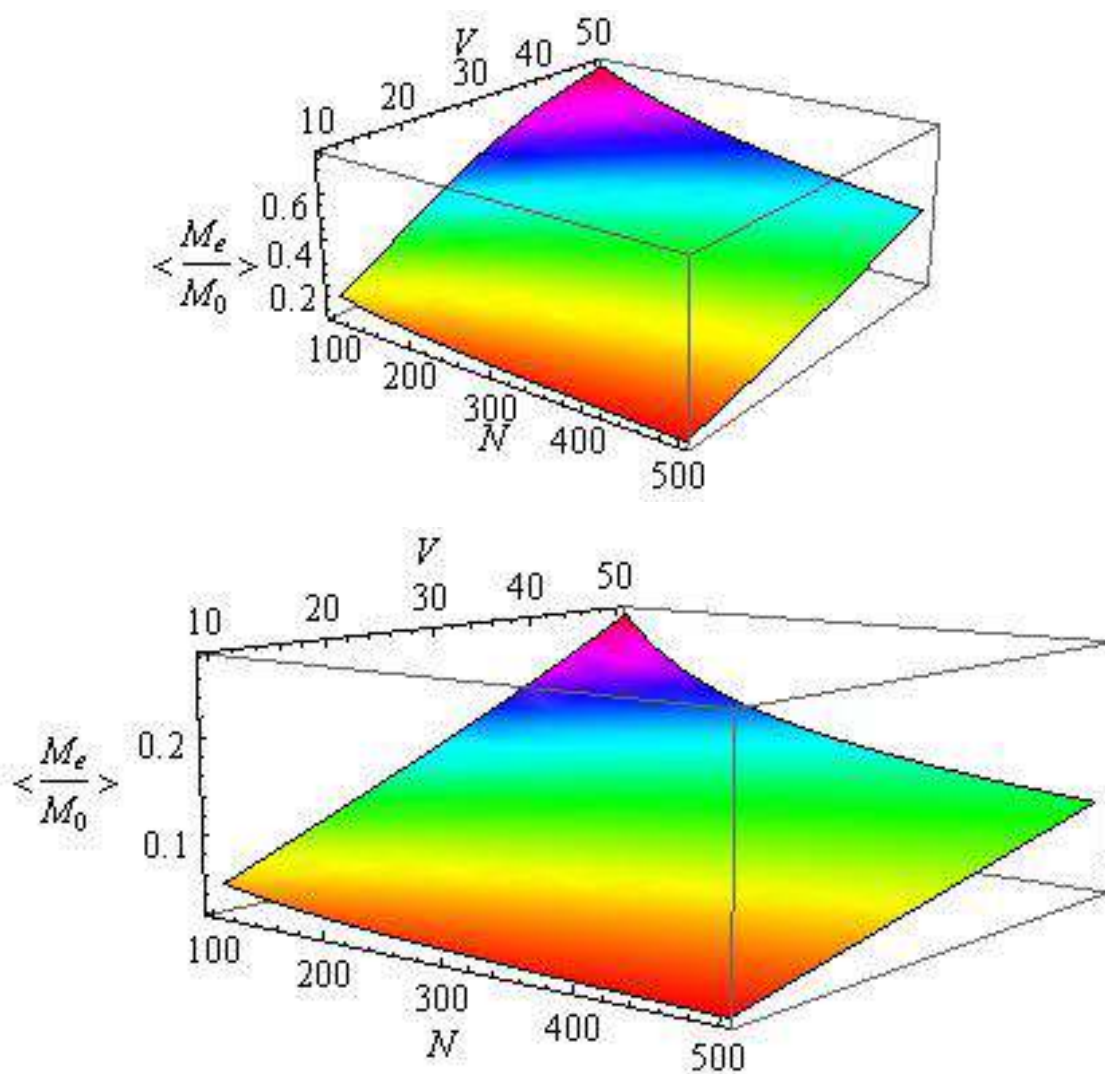


Fig. 9 Time dependence of the averaged normalized magnetization (a) and of $\ln \langle \frac{M_e}{M_0} \rangle$ (b). (c) and (d) demonstrate different time constants of the dependence of $\ln \langle \frac{M_e}{M_0} \rangle$ in different stages of the relaxation: (c) $0 < t < 2$ s and (d) $50\text{s} < t < 100\text{s}$. Here $N=500$, $V=50$ nm³, $F=2$, $\varphi = \pi/2$, $\zeta=1$, $t_c=10^{-5}$ s.

